Archaeological and Anthropological Sciences (2020) 12: 220
https://doi.org/10.1007/s12520-020-01118-x

ORIGINAL PAPER

Networking through pottery characterisation at Takarkori rock shelter (Libyan Sahara, 10,200–4650 cal BP)

Giacomo Eramo[1] · Italo M. Muntoni[2] · Anna Aprile[1] · Mauro Pallara[1] · Rocco Rotunno[3] · Andrea Zerboni[4] · Savino di Lernia[3,5]

Received: 5 January 2020 / Accepted: 16 June 2020 / Published online: 25 August 2020

Abstract

Routine pottery analyses (optical microscopy, X-ray powder diffraction, X-ray fluorescence) and digital image processing of polarised light photomicrographs were used to answer questions on the provenance and technology of pottery assemblages belonging to Late Acacus hunter–gatherers (ca. 10,200–8000 cal BP) and Pastoral herders (ca. 8300–4650 cal BP) from Takarkori rock shelter (SW Libya, central Sahara). This integrated analytical approach on potsherds was combined with the characterisation of local clayey sediments to identify different local and proximal sources for coarse and fine sediments exploited for pottery production. Two main fabric groups (i.e. Q* and QF*) were identified among the analysed potsherds, where the sediments from the Takarkori area are compatible with the quartz-dominated fabrics (Q*). The local fabric QVe shows evidence of dung addition. Pottery with plutonic non-plastic inclusions (QF*) points to provenance from the southern edges of the Tassili n'Ajjer and is more frequent in Late Acacus and Early Pastoral layers. New insights into pottery production and circulation between Early Holocene Saharan hunter–gatherers and Pastoral communities, as well as into modes of occupation of Takarkori rock shelter, are provided.

Keywords Grain size analysis · Point counting · Image analysis · Foragers · Herders · Central Sahara

Introduction

Last decades of archaeological and palaeoenvironmental research in the Sahara highlighted the tight existing correlation between human occupation, environmental changes and the ecology of production (e.g. Cremaschi and di Lernia 1998; Gasse 2000; Wendorf et al. 2007).

It is well known in an anthropological and archaeological perspective how a complete reconstruction of pottery manufacturing processes can contribute to the study of a large array of social and cultural aspects of past human groups (Rye 1981; Arnold 1988; Rice 2015; Roux 2019). In a holistic perspective, key questions are not only the choices made by prehistoric potters but also the conditions under which the potters worked (e.g. Matson 1965; Sillar and Tite 2000; Rice 2015; Duistermaat 2016). In this sense, also climate and environmental conditions may be inferred by various attributes like the presence of gypsum and calcite concretions or degraded vegetal fragments. Moreover, pottery production is also a good indicator of water availability. The long and climate-sensitive time span (ca. 10,200–4650 cal BP) recorded in the archaeological context of Takarkori rock shelter in the Tadrart Acacus Mountains (SW Libya, central Sahara: Fig. 1) provided a lot of data on many aspects of Saharan prehistory from Late Acacus hunter–gatherer–fishers to Late Pastoral herders (e.g. Olmi et al. 2011; Dunne et al. 2012; di Lernia et al. 2012; Biagetti and di Lernia 2013; Cremaschi et al. 2014; Mercuri et al. 2018).

✉ Savino di Lernia
savino.dilernia@uniroma1.it

1 Dipartimento di Scienze della Terra e Geoambientali, Università degli Studi Aldo Moro, Via Orabona, 4, 70125 Bari, Italy

2 Soprintendenza ABAP per le province di BAT e FG, Via Alberto A. Valentini 8, 71121 Foggia, Italy

3 Dipartimento di Scienze dell'Antichità, Sapienza Università di Roma, Piazzale Aldo Moro 5, 00185 Rome, Italy

4 Dipartimento di Scienze della Terra 'A. Desio', Università degli Studi di Milano, Via L. Mangiagalli 34, 20133 Milan, Italy

5 GAES, University of Witwatersrand, Johannesburg, South Africa

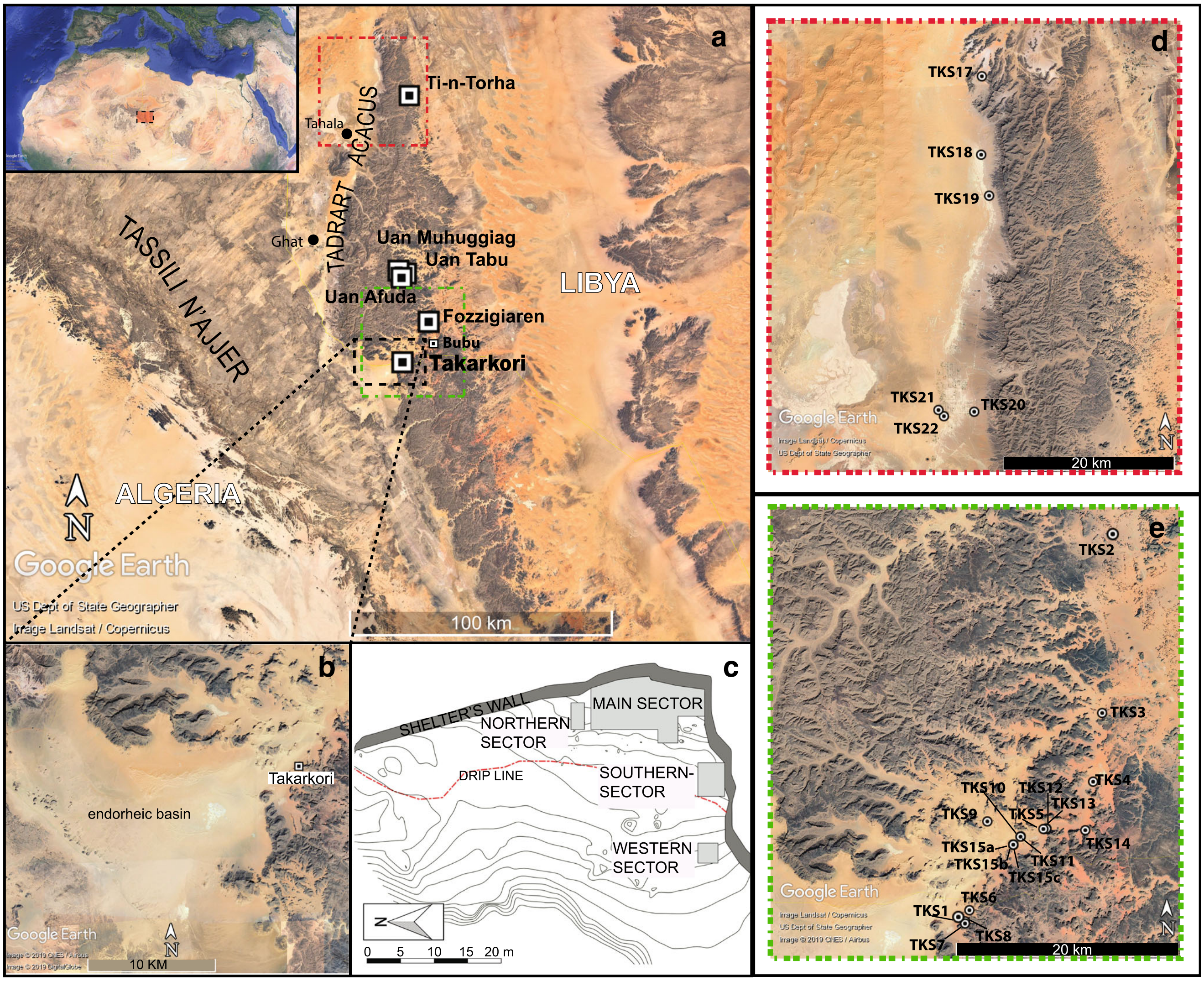

Fig. 1 Map of the Tadrart Acacus area (**a**), with sites discussed in the text. **b** Location of Wadi Takarkori area (dashed rectangle). **c** Simplified plan of the excavations. Insets **d** and **e** indicate the location of geological samplings (see Table 4)

The transitions from Early Holocene foraging acquisitive systems towards food-producing herder communities occurred over the span of several centuries, during which pot-making remains socially situated, reflecting cultural habits, social organisation and ideological meanings. Previous methodological papers (Aprile et al. 2014, 2019; Eramo et al. 2014) on some of the potsherds—here further investigated—gave first insights into provenance and raw material procurement. Quantitative petrographic and morphometric analyses pointed to local wadi/swamp sediments as raw materials for quartz-dominated pottery (Q* fabrics, see below) and a more distant provenance for feldspar-bearing pottery (QF* fabrics, see below), with significant different trends in a chronological perspective. From an ecological point of view, an integrated study of aspects of pottery production, as proposed here, may achieve a better definition of possible raw materials and/or final products' circulation and cultural trajectories.

Takarkori, a key site of Holocene central Sahara

Geological and geomorphological background

The Takarkori rock shelter is positioned on a structural terrace of the southern Tadrart Acacus massif, c. 100 m above the wadi bottom, and opens westwards onto a large shelf floor (Biagetti and di Lernia 2013). The Tadrart Acacus is a sandstone massif located in south-western Libya (Fezzan region, central Sahara), between latitudes 26° N and 24° N (Fig. 2). From the geological point of view, the region belongs to the western fringe of the Murzuq Basin (Desio 1937; Davidson et al. 2000; Ali Kalefa El-ghali 2005), which mainly consists of Palaeozoic sandstone and marls, lying upon the intrusive (granite) formation of the Tassili (Galeĉiĉ 1984; Jakovljevic 1984). The massif consists of Lower to Middle Silurian

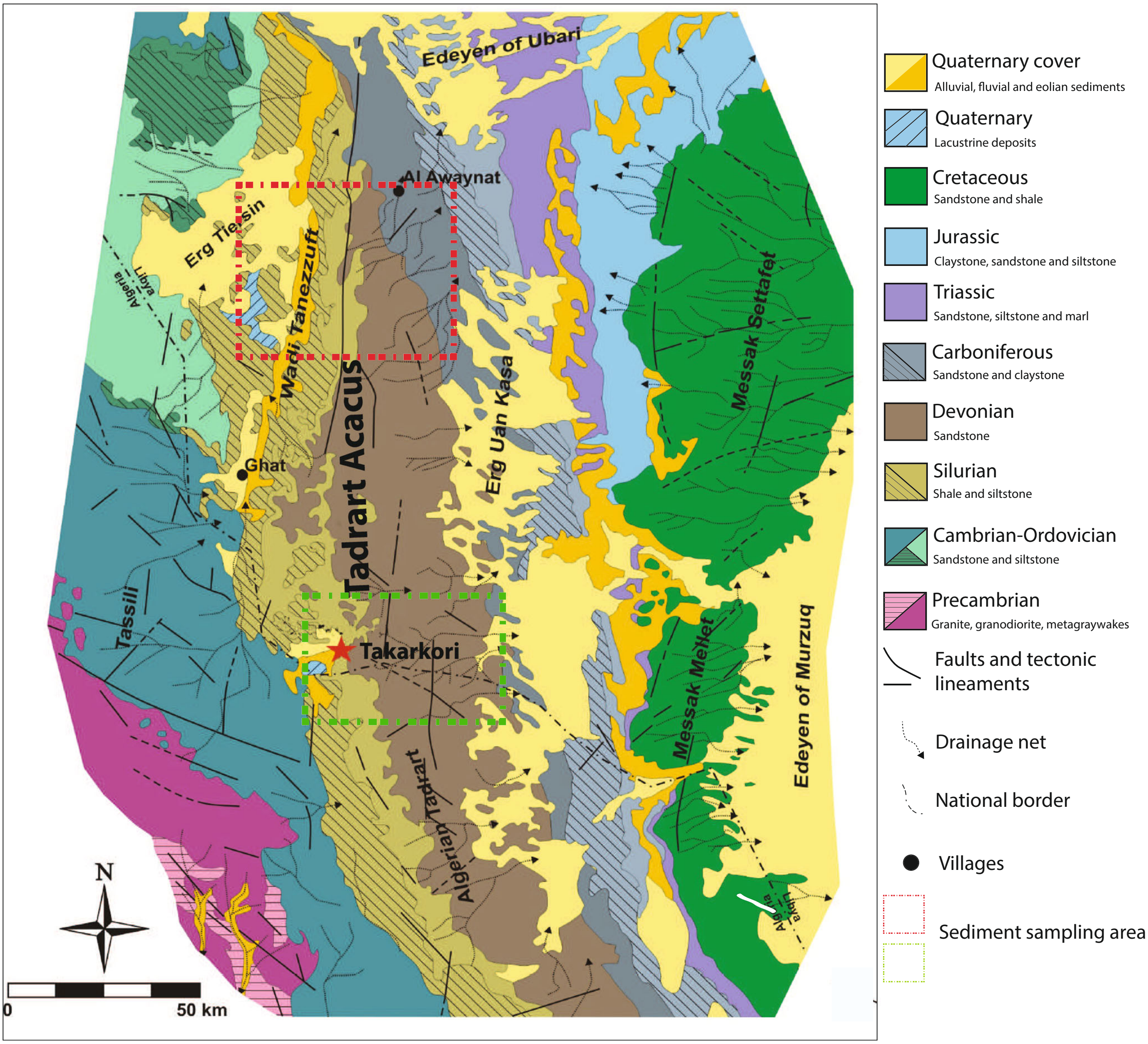

Fig. 2 Simplified geological map of the Tadrart Acacus illustrating the main geological formations; the areas of sampling for sediments (red and green squares as in Fig. 1) and main localities cited in the texts are also indicated (modified from Eramo et al. 2014)

marine shales with sandstone lenses (the Tanezzuft Formation), conformably overlying Upper Silurian and Lower Devonian sandstones of the Acacus and Tadrart formations (Traut et al. 1998; McDougall and Martin 2000; Štorch and Massa 2006). It shows a cuesta-shaped monocline and is delimited to the west by a high scarp. The massif is deeply cut by a dendritic fossil drainage network of W-E-oriented wadis, which consists of deep canyons in their uppermost reaches. The massif has been shaped since the Tertiary by etchplanation and solutional processes, which produced ruiniform landscape and the high number of caves and rock shelters that dot the vertical cliffs of the wadis formed presumably since the Late Neogene, and, at Takarkori, produced an alcove-type rock shelter (Zerboni et al. 2015).

The Wadi Tanezzuft runs for approximately 150 km along the western scarp of the Tadrart Acacus (Cremaschi and Zerboni 2009). Today, the river is dry or at least ephemeral, but in the Holocene, it was a long endorheic fluvial system able to deposit along its course gravel bars and finer sedimentological bodies, consisting of clay and silt.

The Takarkori area corresponds to a pass crossing the Tadrart Acacus massif, separating the Libyan from the Algerian Tadrart. Its southern side consists of a large slope, connecting the upper valley of the Wadi Tanezzuft to the outcrops of the Acacus sandstone. The slope is lined on its northern fringe by large dunes and dotted by some smaller dune systems; the area is covered by a veneer of aeolian sand, except for several outcrops of dark grey clayey sand and fluvial sediments in the lowest part.

Today, the region is hyper-arid, with mean annual temperature between 25 and 30 °C and mean annual rainfall between 0 and 20 mm (Walter and Lieth 1960). During the Early and Middle Holocene (ca. 10,000–5000 cal BP), when the Takarkori rock shelter was occupied, the region experienced higher rainfall triggered by the expansion of the SW African Monsoon domain (Cremaschi and Zerboni 2009). Enhanced rainfall contributed to recharging the local surface aquifers (Cremaschi et al. 2010), sustaining rivers, lakes and a rich plant cover (Mercuri 2008). The wetter phase was interrupted by transitory dry spells (Cremaschi et al. 2010, 2014), and wet environmental conditions ceased due to the progressive reduction in the intensity of the monsoon starting around 5900 cal BP (Cremaschi and Zerboni 2009).

Chronological and cultural background

The multidisciplinary research activity carried out in the last years on the Takarkori rock shelter provided a wealth of information on several aspects on recent Saharan prehistory (e.g. Dunne et al. 2012; Biagetti and di Lernia 2013; Cremaschi et al. 2014; Mercuri et al. 2018).

The well-preserved deposit was excavated between 2003 and 2006 by four sectors covering an area of ~ 140 m^2 by the 'Archaeological Mission in the Sahara' of Sapienza University of Rome and the Department of Archaeology, Tripoli (Fig. 1c). The main sector covers the largest area of investigation (~ 120 m^2), whereas the northern sector (4 m × 2 m) is the only part where the bedrock was reached (depth ~ 1.6 m). The western sector (3 m × 3 m) was located beyond the shelter's drip line, a few metres from the southern sector (5 m × 4 m), which included a stone cairn (Biagetti and di Lernia 2013; di Lernia and Tafuri 2013).

The study area, like much of the central Sahara, enjoyed humid oscillations from the Early to Middle Holocene, with various short and severe dry spells forging the rather unstable palaeoenvironmental context (Mercuri 2008; Cremaschi and Zerboni 2011; Cremaschi et al. 2014).

The stratified sequence is dated from ~ 10,200 to 4650 cal BP, covering the whole Early and Middle Holocene period (Table 1). So far, it is the only site in the Tadrart Acacus to hold physical stratigraphic evidence of the transition from hunting–gathering to early herding and represents an important laboratory for exploring human behaviour and technological developments on a long-term perspective.

The lowermost levels are characterised by a long occupation of hunter–gatherer–fisher groups locally called Late Acacus (LA), radiocarbon dated from ~ 10,200 to ~ 8000 cal BP. Three cultural sub-phases have been identified (LA1, LA2, LA3), also characterised by environmental differences (Biagetti and di Lernia 2013; Cremaschi et al. 2014). Stone structures (huts, platforms, stone rings, etc.), different types of combustion structures (hearths, cuvette-type, ash dumps, etc.) and a complex series of archaeological levels (hardened dung layers, organic sands with plant remains and coprolites, floors, etc.) pertain to this phase, pointing out a rather complex and multifaceted occupation. The subsequent Early Pastoral groups occupied the shelter with their domestic flocks from around ~ 8300 cal BP or slightly later. This phase also is culturally differentiated in two sub-phases (EP1, EP2) and shows aspects of both continuity and change with the previous occupation. Burials became more frequent under the shelter's dome highlighting a shifting pattern from a mere domestic use of the site (di Lernia and Tafuri 2013). Starting at ~ 7100 cal BP, a full herding economy, including dairying (Dunne et al. 2012), is termed Middle Pastoral (MP1, MP2). Developing several centuries, it probably represents the most recognisable prehistoric cultural phase in SW Libya, characterised by specific artefacts and a wide diffusion of archaeological sites. This phase ends with the onset of the present arid conditions, around ~ 5900 cal BP, also marking the beginning of the Late Pastoral. The latter specialised highly mobile ovicaprine herders occupied the shelter seasonally until ~ 5040–4650 cal BP, with more sporadic occupation evidences.

The pottery: formal and decorative patterns

Takarkori pottery shares with other central Saharan Holocene sites several formal and decorative features (e.g. Barich 1974, 1987; Caneva 1987; Aumassip 1984; Roset 1996; Cremaschi and di Lernia 1998; di Lernia 1999; Garcea 2001; Jesse 2010). Late Acacus foragers produced pots with relative thick walls (5–24 mm, mean ~ 10 mm) and dark brown or grey surfaces (from 2.5YR 3/3 to 10YR 3/2) (Fig. 3). Given their high fragmentation, the shape of the vessels is quite difficult to reconstruct, but on the basis of wall orientation and rims, they mostly consist of restricted and unrestricted semi-cylindrical or rounded bowls. Wall fragments are mostly semi-rectilinear or slightly curved, and rims are generally rounded and straight, sometimes flattened. Mouth opening of the vessels inferred from the preserved rims ranges between 18 and 28 cm. The main decoration patterns are represented by the rocker technique, mostly packed zigzags made with an evenly serrated edge instrument. Dotted wavy line motif is present, always in association with the aforementioned packed rocker technique. Undecorated fragments that could also pertain to zonally decorated vessels are common. Rims are mostly decorated with a plain edge rocker stamp either on the lip or on the outer rim part. The Late Acacus assemblage shows in relative few amounts other decorative patterns, like spaced rocker impressions and simple comb impressions.

Significant changes in the pottery production occur with the following Pastoral occupation, in both morphological and stylistic traits. Potsherds are thinner (average ~ 7 mm, from 4 to 11 mm), with more variable wall profiles, ranging

Table 1 Chronology of the main chronocultural phases and their sub-phases identified in the Takarkori area (modified after Cherkinsky and di Lernia 2013, details herein, and in Biagetti and di Lernia 2013)

Phase	Sub-phase	Chronology		
		Years uncal BP	Calibrated years BP (95% confidence)	Calibrated years BC (95% confidence)
Late Pastoral (LP)	LP1	5000–4300	5900–4650	3950–2700
Middle Pastoral (MP)	MP2	5500–5000	6400–5600	4450–3700
	MP1	6100–5500	7100–6200	5200–4250
Early Pastoral (EP)	EP2	6900–6400	7800–7300	5900–5300
	EP1	7400–6900	8300–7600	6400–5700
Late Acacus (LA)	LA3	7900–7400	9000–8000	7050–6100
	LA2	8500–7900	9500–8600	7600–6650
	LA1	8900–8500	10,200–9400	8250–7500

Please note that LP1 at Takarkori is not fully preserved, ending at ca. 4650 cal BP. The calibrated dates express the maximum chronological range, and overlaps are statistically possible. For the calibration, OxCal online (version 4.3) was used (see Ramsey and Lee 2013)

from semi-rectilinear to rounded or very rounded. The few refitted containers pertain to vessels with a short neck or collar and a globular body. Unlike Late Acacus pottery, Pastoral rims are morphologically more varied, with either simple rims undifferentiated (straight or slightly bulging) or fully differentiated (everted or inverted, rounded or flattened) from the wall. The surfaces exhibit a more heterogeneous array of colours, in the range of the reds and browns (ranging from 5YR 3/4 to 10YR 3/4). Finishing treatments include smoothing and burnishing. Yet, the main differences are in the technique and style of decorations, markers of the Pastoral pottery (Caneva 1987). We see a clear shift towards the alternately pivoting stamp (APS) technique: this is characterised by the use of a double-pronged implement in a rocker-like movement resulting in a variety of motifs of various structures. A specific variant of this technique, the 'return' type, albeit of long duration, fully characterised the Middle Pastoral assemblage, as evident in pots decorated by a very regular pattern of rows of dots. Decorative motifs range from paired lines of dots, dashes or triangles, variously arranged on the vessels' body. As being said, other decorative patterns characterise the long Pastoral sequence, and variations are present. Simple impressions with corded instruments are, for instance, restricted to the Early Pastoral, whereas simple burnished pottery characterises the Late Pastoral.

Previous archaeometric studies

Archaeometric analysis of pottery in the Tadrart Acacus region has a long tradition. Palmieri (1987) reports the bulk chemical analyses of 24 sherds coming from different prehistoric sites, dated to three different cultural contexts. The most ancient samples ($n = 8$) are dated to the Late Acacus phase (formerly labelled 'epipalaeolithic ceramic') of three different sites: Uan Muhuggiag ($n = 1$), Fozzigiaren ($n = 5$) and Ti-n-Torha ($n = 2$). All the Middle ($n = 10$) and Late ($n = 6$) Pastoral samples come from Uan Muhuggiag (Fig. 1a). Among the 21 major and trace elements detected by X-ray fluorescence (XRF), 12 were selected as the most significant variables for cluster analysis. The two distinct dendrograms, one considering 7 major elements and the other 5 trace elements, do not show significant groupings, likely given the variability inherent in prehistoric pottery assemblages and also the unbalanced sampling. However, SiO_2 vs. $Na_2O + K_2O$ ratio suggests a sharper cultural–chronological distinction between MP and LA samples, where the increased SiO_2 rate in the former suggests an addition of sand to the clay, while for the LA samples, the low level of SiO_2 indicates the use of a natural clay without any additional temper.

In 1998, Ponti et al. published the analysis of 22 sherds coming from several different prehistoric sites in the Tadrart Acacus and surrounding areas (in Ponti et al. 1998, Fig. 10, they are coded as THA 3, THA 13, THA 14, TH 15-1, TH 15-2, TH 15-3, TH 27-1, TH 27-2, TH 38, TH 42, TH 54, TH 57, TH 84-1, TH 84-2, TH 99, TH 105, TH 111, TH 113, TH 118, UI 5, UI 9 and TAR 3) and of 9 geological samples from local or neighbouring alluvial sediments (Wadi Teshuinat and Wadi Tanezzuft). The XRF and XRD composition appears rather similar for both pottery and soil samples, and the clustering analysis did not identify any grouping related to either spatial distribution or ceramic typology. The 'rocker' pottery group, likely the oldest in terms of typological classification, was probably made of the same clay of the 'Alternated Pivoting Stamp' pottery, of more recent Pastoral phases.

One hundred sixty-nine sherds were collected during the 1960–1963 period. Tinè's excavation at Uan Tabu rock shelter, mainly from Late Acacus layers, was analysed by Livingstone Smith (2001). After a preliminary examination with a low-magnification binocular

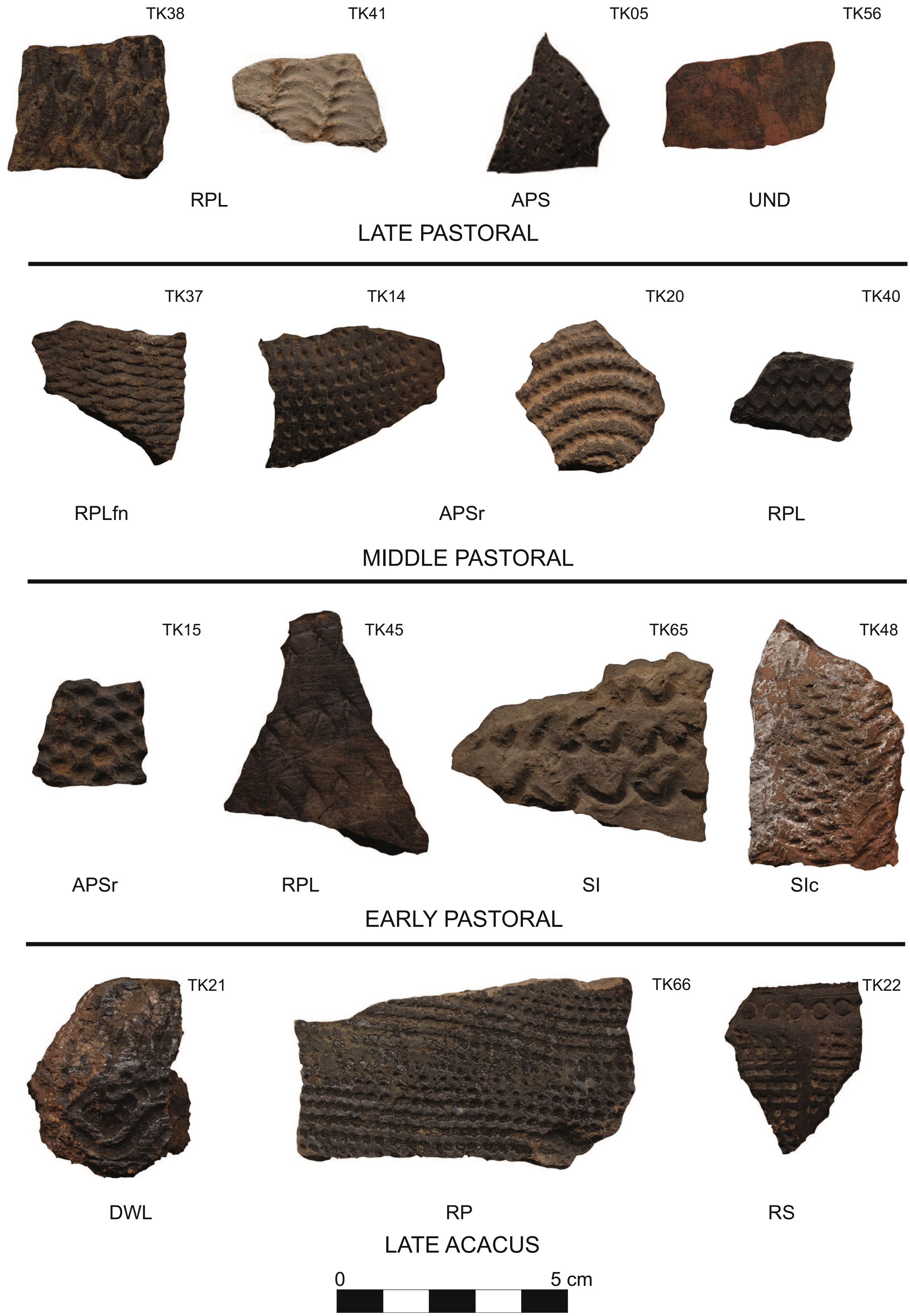

Fig. 3 A selection of potsherds analysed here, by cultural phases (see Table 3 for details). APS, alternately pivoting stamp; APSr, alternately pivoting stamp (return variant); DWL, dotted wavy line; RP, rocker packed; RPL, rocker plain; RPLfn, rocker plain (fish-net variant); RS, rocker spaced (comb); SI, simple impression; SIc, simple impression (corded instrument); UND, undecorated

microscope, six compositional groups (macro-fabrics I to VI) were distinguished. Following this preliminary classification, 22 sherds were analysed by means of standard petrographic thin sections: only two main petrographic fabrics were recognised. The first is a granite-derived group ($n = 17$), which corresponds to I–III macro-fabrics, representing the largest part of the assemblage; the second is a sandstone-derived group ($n = 5$), corresponding to IV–VI macro-fabrics and much less frequent. In the first fabrics, the types of inclusions and their related proportion and morphology suggested that the clay derived from the weathering of a granite or granodiorite formation, probably as eluvial or colluvial sediments. In the second fabrics, the predominance of quartz and the rounded morphology of the grains indicated the use of a compositional and textural mature sediment. Hence, the Author assumed that while the vessels belonging to the sandstone-derived group were locally made at Uan Tabu, those belonging to the granite-derived group were made from materials extracted from more distant sources, likely south-eastern Tassili (ca. 50 km) and carried/exchanged to/with the site of Uan Tabu. Such conclusion has important implications for the understanding of mechanisms of mobility and network within Late Acacus foragers when compared to Pastoral groups.

Aims

On the base of these first indications, this paper aims to (1) identify the petrofacies of the pottery for provenance reconstruction, (2) understand the technological aspects of pottery production and sustainability in a palaeoenvironmental perspective and (3) verify the archaeological hypothesis of pottery circulation in the Tadrart Acacus and surrounding regions.

In order to achieve these aims, the petrographic results on a selection of potsherds from Takarkori previously published (Aprile et al. 2014, 2019; Eramo et al. 2014) are integrated with bulk mineralogical (X-ray powder diffraction (XRPD)) and chemical (XRF) data and compared to those of selected fine local sediments, to test the compatibility of the sedimentary environments inferred from the sedimentological interpretation of the textural and morphometric features of the pottery, with those of the local palaeoenvironmental context. Moreover, statistical analyses applied to the bulk chemical data presented here and to those available from the literature on other analysed pottery fabrics in the region helped to trace out distance correlations and hypothesised trajectories of human groups.

Sampling

Pottery

Approximately 3000 potsherds have been collected from the site (Table 2). Refitting rate is quite low and in a state of preservation poor, as indicated by the average surface of the sherds (~ 18 cm^2). By contrast, organic residues are extraordinarily preserved, as testified by the identification of the earliest direct use for plant processing in the Late Acacus phase (Dunne et al. 2016) and the discovery of Africa's earliest dairying as early as 7100 cal BP (Dunne et al. 2012).

The sampling has been carried out in Libya, and all necessary permission was granted by the Department of Antiquities (DoA) in Tripoli, including destructive analysis, to one of us (SdL). We selected 69 potsherds, based on cultural phase, chronology, stratigraphic context, morphology of the vessel, part of the vessel (rim, neck, wall, base) and type of decoration. The aim was to represent the largest array of cases within an acceptable entity of the sampling (Table 3). Sherds decorated with the APS technique with a double-pronged instrument amount to 20 specimens of which 13 were in the return-type variant. Sixteen sherds present a rocker comb impression with either packed (14) or spaced (2) impression, whereas 1 sherd presents the typical dotted wavy line pattern. Ten sherds are decorated with a rocker plain edge impression and 6 with simple impression, while the remaining are either undecorated (14) or so eroded resulting in an unclear decorative pattern (2): the latter have been kept in order to have a representative sample for the phase LA1. Archaeological contexts too include the variety of deposits recovered in the rock shelter, ranging from the widespread organic sands, whether humified or not, to pits, hearths and stone accumulations.

Local sediments

Several local sediments were sampled (Table 4) in different localities of the Tadrart Acacus massif and along the Wadi Tanezzuft valley as reference to establish the availability and provenance of raw materials (Figs. 1 and 2). Given the position of the shelter—on a pass connecting the upper reaches of the Wadi Tanezzuft valley and the Acacus eastern fringes—we collected geological samples from Late Quaternary deposits deposited on both sides of the massif.

Sandy–silty–clayey sediments accumulated at the bottom of some of the wadis cutting the eastern slope of the Tadrart Acacus massif and others located in the vicinity of the Takarkori rock shelter were also sampled (TKS1–14). These deposits correspond to fluvial sediments accreted possibly in the Upper Pleistocene wet periods. Three samples (TKS15a, TKS15b and TKS15c) were collected in an endorheic depression located behind the Takarkori rock shelter in the locality called Bubu; these samples consist of fine sediments, possibly

Table 2 Numbers of pottery sherds from Takarkori

	Main sector	Northern sector	Western sector	Southern sector	Surface collection	Total
No. of potsherds (samples)	2154 (63)	170 (6)	213 (–)	18 (–)	402 (–)	2957 (69)
LP	173 (7)	– (–)	– (–)	– (–)	36 (–)	– (7)
MP	807 (22)	28 (–)	182 (–)	– (–)	187 (–)	– (22)
EP	632 (19)	16 (1)	– (–)	– (–)	34 (–)	– (20)
LA	507 (15)	126 (5)	23 (–)	18 (–)	29 (–)	– (20)
Unclassified	35 (–)	– (–)	8 (–)	– (–)	116 (–)	– (–)

The number of the samples studied here is presented in parentheses

formed in the Holocene after decantation in a playa to marsh environment. Five samples collected along the Wadi Tanezzuft (TKS18–22) correspond to alluvial sediments formed in the Early or Middle Holocene when the wadi was active. Finally, one sample of the local shales (Tanezzuft Formation) was collected along the Tadrart Acacus outcrops (TKS17).

Analytical methods

Pottery fabric analysis was conducted on thin sections under the polarising microscope Carl Zeiss Axioskop 40 Pol (optical microscopy (OM)). Petrographic description took into account the non-plastic inclusions (NPIs), the matrix and the porosity. The boundary between matrix and NPIs is 15 μm according to Maggetti (1982). Other than the percentage of NPIs, the grain-size distribution (i.e. texture, mode(s)) and the nature of inclusions were considered. The compositional features (e.g. calcareous, ferruginous and micaceous), the presence of clay pellets and the birefringence (e.g. high, medium and low) of the matrix were noted. The structure of the matrix accounts for the oxidation/reduction pattern observed (Fig. 4). This visual scheme classifies the combination of reduced and oxidised domains in the fabric (Eramo and Mangone 2019). The acronyms refer to the sequence of reduced (R) or oxidised (O) domains of the fabric from the core outward. Asymmetric zoning is indicated by adding 'I' (internal) or 'E' (external) at the end of the acronym (ORI = oxidised and then reduced on the inner surface). The 'marbled' (M) structure is characterised by patched reduced and oxidised domains. As for the porosity, primary (i.e. pre-firing) and secondary (i.e. firing-induced) pores were distinguished under the microscope, whereas a quantitative estimation (vol%) was obtained by means of digital image analysis (see below). In order to present a consistent and detailed qualitative description of the fabrics with those of the pottery samples previously published in Eramo et al. (2014), a new classificatory strategy was adopted. The fabric names inform about the most abundant NPIs (prefix) and the nature of the matrix (suffix). As an example, the fabric name 'QVe_io' stands for prevalent quartz (Q) and vegetal inclusions (Ve) in a ferruginous (i) and organic-rich (o) matrix. Other NPI abbreviations are as follows: A = argillaceous rock fragments (ARFs), Ka = carbonate aggregates and F = feldspars (Kfs and/or Pl). Further details about the used methodology are reported in Eramo and Mangone (2019).

Digital image analysis (DIA) techniques using OM images were applied here to estimate the investigated grain size and morphometry of quartz, feldspars and carbonate aggregate inclusions of fabrics QF and QFKa. Image acquisition and segmentation procedure for quartz and carbonate aggregates were performed as described for fabrics Q and QC (QKa in this paper) in Eramo et al. (2014). An appropriate segmentation procedure was instead defined for feldspars (Aprile et al. 2019). As expected, unlike the rare potassium feldspars observed in fabric Q, which were automatically assigned to the background, in fabrics QF and QFKa, quartz and feldspars were contextually segmented according to their well-known optical similarity (Edwards 1916; Deer et al. 1992).

Table 5 shows the volume percentages of matrix and pores estimated by DIA, partially published in Eramo et al. (2014). The ratio $S_{max}/S_{tot} < 0.01$, where S_{max} is the area of the largest inclusion in the four images processed for each thin section and S_{tot} is the sum of the area of four images, assures the same reliability of DIA measurements. The semi-quantitative estimation of the detected components ranges between 0 and 4, indicating absence or their relative amounts.

The range of the equivalent firing temperatures (EFTs, after Tite 1995) was estimated according to the thermal stability ranges (disappearance/appearance) of the mineral phases detected by XRPD. The sintering degree of the analysed potsherds was classified between 'low' and 'medium-high', according to their mineralogical characteristics.

The sediment samples were crushed and quartered to reach the necessary weight (about 50 g) for laboratory analyses. These fractions were put in demineralised water for a complete hydration and to avoid clay aggregates. The grain size analysis was processed in wet condition to obtain a separation by sieving and sedimentation, according to the method

Table 3 Archaeological features of the analysed pottery

Sample	ID	Archaeological context	Chronology	Phases	Max. length (mm)	Max. width (mm)	Thickness (mm)	Decoration
TK01	352	Organic sands	mp	mp2	46	38	4	APS
TK02	1839	Humified organic sands	ep	ep1	32	30	5	APS
TK03	43	Organic sands	mp	mp2	38	34	9	APS
TK04	79	Organic sands	mp	mp2	28	30	6	APS
TK05	283	Organic sands	lp	lp1	39	27	8	APS
TK06	934	Organic sands	mp	mp2	44	40	10	APS
TK07	1825	Organic sands	ep	ep2	42	43	7	APS
TK08	372	Organic sands	mp	mp2	44	18	6	APSr
TK09	412	Organic sands	ep	ep2	34	30	5	APSr
TK10	485	Ash dump	mp	mp1	36	31	4	APSr
TK11	1878	Organic sands	ep	ep2	40	46	5	APSr
TK12	1965	Humified organic sands	ep	ep1	31	25	5	APSr_tr
TK13	60	Organic sands	mp	mp2	28	34	6	APSr
TK14	123	Organic sands	mp	mp2	34	28	7	APSr
TK15	965	Organic sands	ep	ep2	33	32	7	APSr
TK16	1050	Organic sands	ep	ep2	28	24	6	APSr
TK17	1644	Organic sands	mp	mp2	36	34	7	APSr
TK18	582	Organic sands	mp	mp2	36	42	10	APSr
TK19	982	Organic sands	mp	mp2	28	32	10	APSr
TK20	1193	Organic sands	mp	mp2	45	40	6	APSr
TK21	1348	Organic sands	la	la2	44	34	13	DWL
TK22	2605	Organic sands	la	la3	36	30	6	RS
TK23	2191	Hearth	la	la3	42	38	9	RS
TK24	589	Organic sands	mp	mp2	24	31	6	RP
TK25	823	Organic sands	mp	mp2	29	35	8	RP
TK26	964	Humified organic sands	ep	ep1	36	29	6	RP
TK27	166	Organic sands	mp	mp2	40	38	9	RP
TK28	724	Stone accumulation	la	la2	37	28	10	RP
TK29	882	Organic sands	ep	ep2	46	38	7	RP
TK30	1112	Organic sands	ep	ep2	35	49	11	RP
TK31	2082	Organic sands	la	la2	43	43	9	RP
TK32	549	Stone accumulation	la	la2	62	44	12	RP
TK33	717	Stone accumulation	la	la2	41	37	13	RP
TK34	996	Organic sands	ep	ep2	62	49	12	RP
TK35	1324	Organic sands	mp	mp2	62	82	11	RP
TK36	1741	Organic sands	la	la3	37	39	9	RP
TK37	54	Organic sands	mp	mp2	39	28	5	RPLfn
TK38	261	Organic sands	lp	lp1	32	36	6	RPL
TK39	1020	Cemented organic sands	ep	ep2	24	35	5	RPL
TK40	1358	Organic sands	mp	mp2	25	38	6	RPL
TK41	11	Dung	lp	lp1	52	31	11	RPL
TK42	1464	Ash dump	ep	ep2	35	19	11	RPL
TK43	1895	Organic sands	ep	ep2	42	31	11	RPL
TK44	136	Organic sands	mp	mp2	32	30	7	RPL
TK45	1081	Organic sands	ep	ep2	57	75	10	RPL
TK46	1751	Organic sands	la	la3	24	36	8	RPL
TK47	608	Humified organic sands	ep	ep1	43	24	12	SIc
TK48	1850	Humified organic sands	ep	ep1	54	36	9	SIc
TK49	1916	Humified organic sands	ep	ep1	46	40	21	SIc

Table 3 (continued)

Sample	ID	Archaeological context	Chronology	Phases	Max. length (mm)	Max. width (mm)	Thickness (mm)	Decoration
TK50	2047	Organic sands	mp	mp2	40	36	13	SI
TK51	27	Organic sands	mp	mp2	42	35	5	UND
TK52	275	Organic sands	lp	lp1	34	30	4	UND
TK53	400	Organic sands	ep	ep2	59	41	8	UND
TK54	706	Pit (deposit)	lp	lp1	37	29	5	UND
TK55	719	Organic sands	mp	mp2	38	36	6	UND
TK56	1640	Organic sands	lp	lp1	56	34	7	UND
TK57	239	Organic sands	lp	lp1	39	24	7	UND
TK58	572	Stone accumulation	la	la3	68	55	7	UND
TK59	1320	Stone accumulation	la	la3	59	38	7	UND
TK60	1717	Organic sands	la	la3	36	32	9	UND
TK61	807	Stone accumulation	la	la2	62	42	16	UND
TK62	1671	Organic sands	la	la3	35	25	14	UND
TK63	1817	Organic sands	la	la3	45	30	13	UND
TK64	2642	Floor	la	la3	47	47	10	SI-Nabta type[a]
TK65	2653	Organic sands	ep	ep1	41	58	12	SI
TK66	2831	Formal stone structure	la	la1	43	75	8	RP
TK67	2848	Organic sands	la	la1	52	35	9	UNC
TK68	2851	Coarse sand	la	la1	36	21	11	UND
TK69	2852	Coarse sand	la	la1	29	35	7	UNC

ID refers to excavation data. The archaeological context follows a description as in Biagetti and di Lernia 2013

APS alternately pivoting stamp, *APSr* alternately pivoting stamp (return variant), *APSr_tr* alternately pivoting stamp (return variant with triangular impressions), *DWL* dotted wavy line, *RP* rocker packed, *RPL* rocker plain, *RPLfn* rocker plain (fish-net variant), *RS* rocker spaced, *SI* simple impression, *SIc* simple impression (corded instrument), *UNC* unclassifiable, *UND* undecorated

[a] Wolftooth pattern similar to type A1 in Gatto (2002)

proposed by Dell'Anna and Laviano (1987). A distinction among clay (< 2 μm), silt (2–63 μm) and sand (> 63 μm) fractions was obtained.

Seven briquettes of workable local sediments (2 cm × 3 cm × 1 cm) were hardened at 400 °C for 1 h in an electric kiln to ease the preparation of the thin sections, without important mineralogical alterations. Their petrographic description followed the above-mentioned criteria, except for porosity.

A portion of ceramic samples between 5 and 10 g was used for bulk mineralogical and chemical analyses after mechanical elimination of surface portion and encrustations. It was then powdered for 8 min at a frequency of 10 Hz in the vibratory ball mill Retsch MM 400 equipped with two 25-ml tungsten carbide grinding jars with two tungsten carbide balls of 1.5 cm in diameter. About 1 g of powder from each sample was investigated by means of XRPD. A PANalytical X'Pert MRD diffractometer equipped with a PANalytical X'Celerator detector and Cu Kα radiation was used. The X-ray tube was operated at 40 kV and 40 mA, and spectra in the 2–65° 2θ angular range were recorded. All XRPD spectra were processed with the X'Pert HighScore software (PANalytical, version 3.0), with a PDF-2 reference database (ICDD) for identification of inorganic phases.

The bulk chemical analysis of the potsherds and local clays was performed by an automatic spectrometer Panalytical AXIOS-Advanced, equipped with the X-ray tube X SST-mAX (Rh anode).

Concentrations of major and minor oxides and trace elements were determined on pressed powder pellets after the analytical techniques outlined elsewhere (Franzini et al. 1972; Franzini 1975; Leoni and Saitta 1976). The limit of detection for major element oxides was 0.01 wt%, and that for trace elements was about 10 ppm. The accuracy was checked with two international standards (AGV-1 of USGS-USA and NIM-G of NIM-South Africa). Loss on ignition (LOI) was determined by heating the samples at 1000 °C for 12 h.

The petrographical and chemical data were processed and drawn by PAST 3 (Hammer et al. 2001).

In order to compare the XRF data of the potsherds and sediments studied here with those of other samples from different archaeological contexts in the region (Palmieri 1987; Ponti et al. 1998), the concentrations of the major and minor oxides of each sample, except for P_2O_5 and CaO potentially altered by contamination, were normalised on SiO_2 values, to make comparable data of different laboratories. Multivariate statistical analysis was applied to the chemical data for a better

Table 4 Position and major geological properties of local samples of sediment

Sample	Coordinates	Location of sampling point	Type of sediment	Age of deposition	Colour of the deposit
TKS1	24° 31′ 23.6″ N, 10° 31′ 01″ E	Outcrop along a small wadi southward of Takarkori rock shelter	Medium coarse alluvial sediment at the bottom of the wadi	Pleistocene/Holocene	2.5YR 5/8
TKS2	24° 49′ 35.4″ N, 10° 39′ 05.2″ E	Outcrop in the area called Imenaneia, north of Takarkori rock shelter	Medium coarse alluvial sediment at the bottom of the wadi	Pleistocene/Holocene	2.5YR 5/8
TKS3	24° 41′ 04.4″ N, 10° 38′ 31.3″ E	Outcrop in the area called Fozzigiaren, north of Takarkori rock shelter	Medium coarse alluvial sediment at the bottom of the wadi	Pleistocene/Holocene	2.5YR 5/8
TKS4	24° 37′ 48.7″ N, 10° 38′ 02.7″ E	Outcrop along Wadi Bubu, east of Takarkori rock shelter	Slightly laminated alluvial sediment at the bottom of the wadi	Pleistocene/Holocene	7.5YR 6/6
TKS5	24° 35′ 33.9″ N, 10° 35′ 26.7″ E	Outcrop in the area between Wadi Bubu e Wadi Afar, north-east of Takarkori rock shelter	Slightly laminated alluvial sediment at the bottom of the wadi	Pleistocene/Holocene	7.5YR 6/6
TKS6	24° 31′ 42.7″ N, 10° 31′ 35.2″ E	Outcrop along a small wadi southward of Takarkori rock shelter	Slightly laminated alluvial sediment at the bottom of the wadi	Pleistocene	2.5YR 5/8
TKS7	24° 31′ 04.5″ N, 10°31′ 21.4″ E	Outcrop along a small wadi southward of Takarkori rock shelter	Slightly laminated alluvial sediment at the bottom of the wadi	Pleistocene	7.5YR 6/6
TKS8	24° 31′ 11″ N, 10° 31′ 21.4″ E	Outcrop along a small wadi southward of Takarkori rock shelter	Slightly laminated alluvial sediment at the bottom of the wadi	Pleistocene	2.5YR 5/8
TKS9	24° 35′ 55.4″ N, 10° 32′ 30.9″ E	Outcrop along Wadi Afar, north of Takarkori rock shelter	Slightly laminated alluvial sediment at the bottom of the wadi	Pleistocene	7.5YR 6/8
TKS10	24° 35′ 11.9″ N, 10° 34′ 15.2″ E	Outcrop in the area between Wadi Bubu e Wadi Afar, north-east of Takarkori rock shelter	Slightly laminated alluvial sediment at the bottom of the wadi	Pleistocene/Holocene	2.5YR 6/1
TKS11	24° 35′ 12.7″ N, 10° 34′ 15.9″ E	Outcrop in the area between Wadi Bubu e Wadi Afar, north-east of Takarkori rock shelter	Slightly laminated alluvial sediment at the bottom of the wadi	Pleistocene/Holocene	7.5YR 6/6
TKS12	24° 35′ 35.4″ N, 10° 35′ 36″ E	Outcrop along Wadi Bubu, east of Takarkori rock shelter	Slightly laminated alluvial sediment at the bottom of the wadi	Pleistocene	2.5YR 5/1
TKS13	24° 35′ 34.6″ N, 10° 35′ 35.7″ E	Outcrop along Wadi Bubu, east of Takarkori rock shelter	Slightly laminated alluvial sediment at the bottom of the wadi	Pleistocene	2.5YR 6/8
TKS14	24° 35′ 30.4″ N, 10° 37′ 38.4″ E	Outcrop along Wadi Bubu, east of Takarkori rock shelter	Slightly laminated alluvial sediment at the bottom of the wadi	Pleistocene	2.5YR 5/8
TKS15a	24° 34′ 48.9″ N, 10° 33′ 52.6″ E	Outcrop in the middle of a depression along Wadi Bubu, east of Takarkori rock shelter	Alluvial/marsh deposit (endorheic delta facies)	Early/Middle Holocene	5YR 6/8
TKS15b	24° 34′ 48.9″ N, 10° 33′ 52.6″ E	Outcrop in the middle of a depression along Wadi Bubu, east of Takarkori rock shelter	Alluvial/marsh deposit (endorheic delta facies)	Early/Middle Holocene	2.5YR 5/1
TKS15c	24° 34′ 48.9″ N, 10° 33′ 52.6″ E	Outcrop in the middle of a depression along Wadi Bubu, east of Takarkori rock shelter	Alluvial/marsh deposit (endorheic delta facies), rich in organic matter	Early/Middle Holocene	2.5YR 4/1
TKS17	25° 45′ 59.1″ N, 10° 23′ 00.1″ E	Outcrop along Wadi Tanezzuft, north-west of Takarkori rock shelter	Alluvial deposit	Middle Holocene	7.5R 5/8
TKS18	25° 41′ 03.3″ N, 10° 22′ 57.6″ E	Outcrop along Wadi Tanezzuft, north-west of Takarkori rock shelter	Alluvial deposit	Middle Holocene	7.5R 5/8
TKS19	25° 38′ 28.8″ N, 10° 23′ 31.2″ E	Outcrop along Wadi Tanezzuft, north-west of Takarkori rock shelter	Alluvial deposit	Middle Holocene	7.5R 5/8
TKS20	25° 24′ 52.8″ N, 10° 22′ 30.6″ E		Alluvial deposit	Middle Holocene	7.5R 6/8

Table 4 (continued)

Sample	Coordinates	Location of sampling point	Type of sediment	Age of deposition	Colour of the deposit
		Outcrop in the village of Tahala, along Wadi Tanezzuft, north-west of Takarkori rock shelter			
TKS21	25° 24′ 59″ N, 10° 20′ 01.2″ E	Outcrop in the village of Tahala, along Wadi Tanezzuft, north-west of Takarkori rock shelter	Alluvial deposit	Middle Holocene	7.5R 6/8
TKS22	25° 24′ 35.4″ N, 10° 20′ 24.2″ E	Outcrop in the village of Tahala, along Wadi Tanezzuft, north-west of Takarkori rock shelter	Alluvial deposit	Middle Holocene	7.5R 5/8

Colours were defined according to the Munsell soil colour chart code (Munsell Color Company 1975)

understanding of the existing correlations among variables of each dataset. For the principal component analysis (PCA), the normalised data were then standardised to ensure the normal distribution and the same variance ($\mu = 0$; $\sigma = 1$) (Davis 1986, p. 517).

Results

Pottery

Petrography and mineralogy

Sixty-nine potsherds are classifiable in six fabrics on the basis of the prevailing NPIs and microstructures (Table 5). Moreover, according to the characterising presence of feldspars, the six fabrics were ascribed to two groups: Q* (Q, QVe, QA, QKa) and QF* (QF, QFKa). There is no petrographical evidence for secondary carbonates and/or phosphates in the open pores and/or of concretions on the surface.

All the potsherds show carbonate-free matrix, with carbonaceous matter more or less preserved according to the dynamics of firing.

The NPIs are characterised by the presence of monocrystalline quartz, with less common polycrystalline quartz (Fig. 5a, b). Plagioclase is rare or absent, except in QF and QFKa (QF*). A prevalent andesine composition (30–50% An) was optically estimated. The K-feldspars occur in QF* fabrics as orthoclase and rarely as microcline (e.g. TK68). As a whole, plagioclase crystals are more altered than K-feldspars. Hornblende is also present in QF* fabrics, sometimes present in plutonic lithic fragments, associated to quartz and feldspars, as well as fair amounts of biotite (partly chloritised) and traces of epidote (Table 5).

The XRPD of the powdered potsherds essentially confirmed the mineralogical observation made under the polarising microscope and added new details about the fine-textured fraction present in the matrix. The samples of Q* fabrics show prevalent quartz and sometimes traces of K-feldspars. The basal peak (100) of illite/muscovite and the cumulative peak of clay minerals at 4.5 Å are always present. Minor amounts of smectite and kaolinite were also detected. As for the QF* fabrics, the K-feldspars are generally more abundant than plagioclase, and some chlorite was detected, other than biotite.

Fabric group Q* Monocrystalline quartz with unit and undulose extinction is characteristic of fabric Q, with rare polycrystalline plutonic quartz. Few muscovite crystals are dispersed in the ferruginous matrix, where always presents a relic carbonaceous matter. Only in TK43 were detected few K-feldspars.

Table 5 Petrographical (OM) and mineralogical (XRPD) outline of the pottery fabrics

Sample	Phases	Fabric	Matrix					Porosity		Non-plastic inclusions																EFT (°C)	Sintering
			Composition	cp	Birefringence	Structure	vol%*	vol%*	Porosity type	Qm	Qp	Pl	Kfs	Hbl	Bt	Ill/ Ms	Chl	Kln	Sme	Ep	Ka	SRF	ARF	Ia	Ve		
TK01	mp2	QVe	io	0	M	RO	85.11	7.66	I, II	4	0	1	0	0	0	3	0	0	0	0	0	0	0	2	3	600–800	M
TK02	ep1	QKa	io	0	L	RO (M)	70.80	6.82	(I), II	4	0	1	1	0	0	1	0	0	2	0	2	0	0	2	0	700–900	MH
TK03	mp2	QKa	io	0	M	M	70.47	5.11	I, II	4	0	1	0	0	0	2	0	0	2	0	2	0	0	2	0	600–800	M
TK04	mp2	QA	io	0	M	ROE	69.70	3.99	I, (II)	4	0	1	0	0	0	2	0	0	0	0	0	0	3	3	0	600–800	M
TK05	lp1	Q	io	1	M	RO (M)	76.28	4.48	I, II	4	1	1	0	0	0	2	0	0	1	0	0	0	0	2	1	600–800	M
TK06	mp2	QVe	io	0	M	ROE	70.83	4.58	I, II	4	0	0	0	0	0	2	0	2	0	0	0	0	0	2	2	500–700	ML
TK07	ep2	QKa	io	0	MH	RO	69.65	5.84	I, II	4	1	0	1	0	0	1	0	0	2	0	2	0	0	2	2	700–900	MH
TK08	mp2	QF	mo	0	M	ROI	74.05	4.14	(I), II	3	2	2	3	1	3	1	0	0	0	0	0	0	0	2	0	600–800	M
TK09	ep2	QKa	io	0	H	RO	78.45	4.17	(I), II	4	1	1	1	0	0	2	0	0	0	0	1	0	0	2	1	600–800	M
TK10	mp1	QVe	io	0	MH	RO	85.46	3.80	I, II	4	1	0	0	0	0	3	2	0	0	0	0	0	0	2	2	500–700	L
TK11	ep2	Q	io	0	nd	R	73.52	4.21	(I), II	4	1	0	0	0	0	2	0	2	2	0	0	0	0	2	1	500–700	ML
TK12	ep1	QF	io	0	nd	R	74.64	4.09	(I), II	3	2	2	3	1	4	1	0	0	2	1	0	0	0	2	1	600–800	M
TK13	mp2	Q	io	0	M	RO	70.38	5.28	(I), II	4	1	0	0	0	0	1	0	1	1	0	0	0	0	2	1	600–800	M
TK14	mp2	Q	io	0	L	ROI	78.72	4.88	I, II	4	0	1	0	0	0	2	0	0	2	0	0	0	0	2	0	600–800	MH
TK15	ep2	QVe	io	0	M	RO	75.40	7.36	I, II	4	1	1	0	0	0	3	0	0	2	1	0	0	0	2	3	600–800	M
TK16	ep2	QKa	io	0	H	ROE	78.06	4.53	(I), II	4	1	1	1	0	0	3	0	2	0	0	1	0	0	2	1	500–700	ML
TK17	mp2	QVe	io	0	M	RO	77.83	4.97	I, II	4	0	0	0	0	0	3	0	0	2	0	0	0	0	2	2	600–800	M
TK18	mp2	QKa	io	0	M	O (M)	68.23	4.68	(I), II	4	1	0	1	0	0	2	0	0	2	1	1	1	0	2	0	600–800	M
TK19	mp2	QKa	io	0	M	RO	65.39	7.46	(I), II	4	1	1	1	1	0	2	0	0	2	1	2	0	0	2	0	600–800	M
TK20	mp2	QF	mo	0	M	ROE	71.05	7.10	(I), II	3	2	2	3	1	3	1	0	0	0	0	0	1	0	2	0	600–800	M
TK21	la2	QF	mo	0	MH	O (M)	86.12	2.94	(I), II	3	2	2	3	1	3	1	3	0	0	1	0	0	0	2	2	600–800	ML
TK22	la3	QKa	io	0	L	ROE	69.38	4.68	(I), II	4	0	1	0	0	0	2	0	0	2	1	2	0	0	2	0	600–800	MH
TK23	la3	QF	mo	0	L	R	78.66	8.28	(I), II	2	3	2	3	0	4	1	0	0	1	1	0	1	0	2	1	600–800	MH
TK24	mp2	Q	io	0	M	R	80.51	4.67	(I), II	4	1	1	1	0	0	2	0	0	2	0	0	0	0	2	1	500–700	ML
TK25	mp2	QKa	io	0	nd	R	72.55	2.77	(I), II	4	1	1	1	1	0	2	0	0	2	1	2	0	0	2	2	600–800	M
TK26	ep1	Q	io	0	MH	ROE	70.54	3.77	I, II	4	1	0	1	0	0	1	0	0	1	0	0	0	0	2	1	600–800	M
TK27	mp2	QA	io	0	M	RO	69.99	4.36	(I), II	4	2	1	1	1	0	2	0	0	2	0	0	0	2	2	2	600–800	M
TK28	la2	QF	mo	0	MH	R (M)	78.33	3.50	I, II	3	2	2	2	0	3	1	2	0	0	1	1	0	0	2	1	600–800	ML
TK29	ep2	QKa	io	0	MH	ROE	80.81	7.00	(I), II	4	1	1	1	0	0	2	0	0	2	0	1	0	0	2	1	600–800	M
TK30	ep2	QKa	io	0	ML	ROE	71.67	5.42	I, II	4	1	1	1	0	0	1	2	0	2	0	1	0	0	2	1	700–900	MH
TK31	la2	QFKa	mo	0	H	O	74.77	7.00	(I), II	3	2	1	3	1	4	0	3	0	0	0	1	0	0	2	0	500–700	ML
TK32	la2	QF	mo	0	MH	ROI (M)	72.90	6.70	(I), II	3	2	2	2	2	3	0	0	0	1	0	0	0	0	2	2	600–800	ML
TK33	la2	QF	mo	0	M	O (M)	80.41	6.43	(I), II	2	2	2	3	1	3	1	1	0	0	1	0	0	0	2	2	600–800	MH
TK34	ep2	QVe	io	1	H	RO (M)	87.10	7.57	I, II	3	1	1	0	0	0	3	0	0	0	0	0	0	0	2	3	600–800	M
TK35	mp2	QF	mo	0	M	RO	70.88	8.94	I, II	3	2	2	3	1	2	0	2	0	0	0	0	1	0	2	1	500–700	ML
TK36	la3	QF	mo	0	M	R (M)	77.89	3.46	I, II	3	2	2	3	0	3	0	2	0	1	1	0	0	0	2	0	500–700	ML
TK37	mp2	QVe	io	0	M	RO	81.19	3.27	(I), II	4	1	1	1	0	0	3	0	2	0	1	0	0	0	2	2	500–700	ML
TK38	lp1	QVe	io	0	M	ROE	73.54	5.62	(I), II	4	1	1	0	0	0	1	0	0	1	0	0	0	0	2	2	700–900	MH
TK39	ep2	QVe	io	0	M	RO	75.23	2.01	I, II	4	1	1	0	0	0	1	0	0	1	0	0	1	0	2	2	700–900	MH
TK40	mp2	QKa	io	0	M	ROI	78.50	3.70	(I), II	4	1	0	1	0	0	2	0	0	2	0	1	0	0	2	2	600–800	M
TK41	lp1	QF	mo	0	M	RO (M)	75.74	2.92	(I), II	3	2	2	3	0	3	1	0	0	1	0	0	0	0	2	0	600–800	M
TK42	ep2	QF	mo	0	M	R	73.23	6.84	(I), II	3	2	2	3	0	3	0	0	0	1	1	0	0	0	2	0	600–800	M
TK43	ep2	QVe	io	0	M	M	77.83	4.61	I, II	3	1	1	1	0	0	4	0	3	2	0	1	0	0	2	3	500–700	L
TK44	mp2	QF	mo	0	ML	ROE	77.92	3.60	(I), II	3	2	2	3	2	3	1	2	0	1	0	0	0	0	2	1	600–800	MH
TK45	ep2	QF	mo	0	M	RO	78.80	8.43	I, II	3	2	2	3	1	2	2	0	0	1	0	0	0	0	2	2	600–800	M
TK46	la3	QF	mo	0	MH	RO	77.88	5.95	I, II	3	2	2	3	1	3	1	0	0	0	0	1	0	0	2	2	600–800	ML
TK47	ep1	QF	mo	1	H	O (M)	80.55	5.90	(I), II	3	2	1	3	0	4	1	0	0	0	1	0	0	0	2	2	600–800	ML
TK48	ep1	QF	mo	0	H	ROI	80.46	5.70	(I), II	3	2	1	3	0	3	1	0	0	1	1	0	0	0	2	0	600–800	ML
TK49	ep1	QF	mo	0	MH	R	73.49	4.18	I, II	3	2	1	3	0	3	1	1	0	0	0	0	0	0	2	1	500–700	ML
TK50	mp2	QF	mo	0	M	ROI	80.94	2.11	I, II	2	3	2	3	0	4	1	0	0	0	0	0	0	0	2	1	600–800	M

Table 5 (continued)

Sample	Phases	Fabric	Matrix					Porosity		Non-plastic inclusions																EFT (°C)	Sintering
			Composition	cp	Birefringence	Structure	vol%*	vol%*	Porosity type	Qm	Qp	Pl	Kfs	Hbl	Bt	Ill/ Ms	Chl	Kln	Sme	Ep	Ka	SRF	ARF	Ia	Ve		
TK51	mp2	Q	io	0	M	ROI	73.85	3.60	(I), II	4	0	1	2	0	0	1	0	0	0	1	1	0	0	2	0	600–800	M
TK52	lp1	QVe	io	0	M	ROI	86.97	5.51	I, II	4	1	1	1	0	0	2	0	0	0	0	0	1	0	2	2	600–800	M
TK53	ep2	QKa	io	0	L	RO	71.65	4.29	(I, II)	4	0	0	0	0	0	1	0	0	0	0	1	0	0	2	1	700–900	MH
TK54	lp1	QVe	io	0	MH	ROI	79.44	3.37	(I), II	4	0	1	0	0	0	2	0	0	1	0	1	0	0	2	2	600–800	ML
TK55	mp2	QVe	io	0	M	RO	74.24	4.34	I, II	4	1	1	0	0	0	2	0	0	1	0	0	0	1	2	3	600–800	M
TK56	lp1	QKa	io	0	L	RO	75.91	5.82	I, (II)	4	0	1	0	0	0	1	0	0	0	1	1	0	0	2	0	700–900	MH
TK57	lp1	Q	io	0	M	ROE	71.85	5.07	I, II	4	1	0	1	0	0	2	0	2	2	0	0	0	0	3	0	500–700	ML
TK58	la3	QF	mo	0	M	ROE	77.13	4.39	(I, II)	3	2	2	4	0	2	0	0	0	0	1	0	1	0	2	0	600–800	M
TK59	la3	QF	mo	0	M	RO (M)	76.02	3.83	(I), II	3	1	2	4	0	2	1	0	0	1	0	0	0	0	2	0	600–800	M
TK60	la3	QF	mo	0	MH	ROI	78.14	6.87	I, (II)	2	2	2	4	1	4	1	0	0	1	1	0	0	0	2	0	600–800	ML
TK61	la2	QF	mo	0	M	ROE	76.48	4.25	(I), II	2	2	1	4	0	4	1	0	0	1	1	0	0	0	2	1	600–800	M
TK62	la3	QF	mo	0	H	ROI (M)	72.28	8.66	(I), II	3	2	1	3	0	3	0	0	0	1	1	0	0	0	2	1	600–800	ML
TK63	la3	QF	mo	0	H	RO	77.85	4.66	(I), II	3	2	1	3	0	4	0	0	0	1	1	0	0	0	2	2	600–800	ML
TK64	la3	QF	mo	0	M	RO	82.92	6.15	(I), II	2	2	2	4	1	4	1	0	0	1	1	0	0	0	2	1	600–800	M
TK65	ep1	QF	mo	0	M	ROI (M)	90.50	3.14	(I), II	3	2	1	2	1	4	0	0	0	1	1	0	0	0	2	2	600–800	M
TK66	la1	QFKa	mo	0	M	RO (M)	80.01	5.04	I, II	3	2	2	3	1	4	1	0	0	1	1	2	0	0	2	2	600–800	M
TK67	la1	QF	mo	0	M	ROE	76.24	7.52	(I), II	3	2	2	3	1	0	2	0	0	1	1	0	0	0	2	2	600–800	M
TK68	la1	QF	mo	0	H	ROE	89.95	2.80	(I), II	3	2	2	3	0	3	1	0	0	2	1	0	0	0	2	0	600–800	ML
TK69	la1	QFKa	mo	0	MH	M	75.75	2.03	(I), II	3	2	2	3	1	3	1	2	0	0	1	2	0	0	2	1	500–700	ML

Parentheses indicate minor amounts; 0–4 indicate relative amounts

Qm monocrystalline quartz, *Qp* polycrystalline quartz, *Pl* plagioclase, *Kfs* K-feldspars, *Ill/Ms* muscovite, *Hbl* hornblende, *Ep* epidote, *Bt* biotite, *Chl* chlorite, *Kln* kaolinite, *Sme* smectite, *SRF* sedimentary rock fragments, *ARF* argillaceous rock fragments, *Ia* ferruginous aggregates, *Ka* carbonate aggregates, *Ve* vegetal inclusions, *io* iron oxides-oxyhydroxides, *mo* micaceous organic matter, *cp* clay pellets, *I* primary porosity, *II* secondary porosity, *L* low, *M* medium, *H* high, *nd* non detectable

*Data obtained by DIA (see text), partially presented in Eramo et al. (2014)

Carbonised organic inclusions such as stems and grains are frequent in fabric QVe (Fig. 5d).

The matrix structure is essentially zoned in both fabric groups, with symmetric (RO) or asymmetric (ROI, ROE, M) oxidation pattern parallel to the surfaces of the potsherds (Fig. 4). A complete reduced structure (R) occurs in TK11 and TK24. A medium birefringence of the matrix is the rule, with few cases of low and high birefringence in QKa (Table 5).

The secondary porosity is quite prevalent in fabric Q and equivalent to primary porosity in fabric QVe (Table 5).

The two samples ascribed to fabric QA (TK4, TK27) feature the presence of mudstone fragments (ARF) (Fig. 5c). Some microcrystalline carbonate aggregates (Ka) occur as NPIs in fabric QKa (Fig. 5g).

Fabric group QF* The petrofacies of fabrics QF and QFKa is clearly distinguishable from that of Q and QKa, because of the presence of K-feldspars and plagioclase, along with minor amounts of biotite and hornblende, other than monocrystalline and polycrystalline quartz (Fig. 5e, f). Moreover, the NPIs in fabrics QF and QFKa are more angular than those of fabrics Q and QKa (see below). The carbonate aggregates, occurring in QFKa, cement iron oxides and quartz grains (Fig. 5h).

The matrix presents high optical density due to carbonaceous matter, often partially oxidised near the external surfaces (RO*). Complete oxidation (O) never occurs whereas complete reduction (R) was observed in four samples (Table 5). Secondary pores related to the partial combustion of vegetal inclusions and organic matter are prevalent (Fig. 5d, e).

Texture and morphometry

Grain size and morphometric data obtained by DIA for quartz (Qz), feldspars (Fsp) and calcareous aggregates (Ka) of fabrics QF and QFKa are presented separately. The normalised grain-size distributions for these fabrics are reported in Table 6. Corresponding statistical parameters (both graphic and moment methods) are shown in Table 7. The morphometric data obtained are reported as median value for each grain-size class in Table 8.

Quartz According to graphic statistical parameters (computed as overall datum), both quartz grain-size distributions of fabrics QF and QFKa are defined as poorly sorted and platykurtic. However, the former is positively skewed while the latter is symmetrical. Moreover, a prevalence of the 500-μm class (coarse sand) is observed for QF while a prevalence of the 125–250-μm class (fine sand) is recorded for QFKa. The overall volume percentage of quartz is quite similar for both fabrics, that is 8.79% for QF and 9.27% for QFKa.

The grain-size distributions for both fabrics appear highly variable, even if only three samples belong to fabric QFKa. Actually, the mean Mz values range between 0.83Φ and 3.76Φ for QF and the value was 1.87Φ for sample TK69 and 2.23Φ for sample TK66 of QFKa. Generally, variability was recorded mostly for 1Φ and 3Φ classes for the former and for 2Φ and 4Φ classes for the latter.

Eventually, both fabrics show a broad tendency to bimodality, as for samples TK28, TK45, TK49 and TK68 of fabric QF and TK69 of fabric QFKa. Samples TK12, TK20 and TK50 of fabric QF appear even strongly bimodal.

Considering the morphometric results, a weak tendency to circularity and moderate to elongation are shown in both fabrics. Particularly, quartz inclusions of QF are more elongated than those of QFKa. As far as roundness and rectangularity are concerned, quartz inclusions for both fabrics are described as sub-angular and sub-rounded grains with a square shape.

Feldspars Feldspar grain-size distributions for both fabrics QF and QFKa are described as poorly sorted and mesokurtic on the base of the graphic statistical parameters computed as overall datum. However, the former is very positively skewed while the latter is positively skewed. Furthermore, a prevalence of the 500 μm class (coarse sand) is observed for QF while a prevalence of the 250–500 μm class (medium sand) is recorded for QFKa. The overall volume percentage of feldspars is quite similar for both fabrics, that is 7.21% for QF and 5.40% for QFKa.

As well as for quartz of the same fabric, the grain-size distributions of feldspars for fabrics QF and QFKa appear generally variable since the mean Mz values range between 0.90Φ and 2.65Φ for QF while Mz is 1.99Φ for sample TK66 and 3.17Φ for TK69 of fabric QFKa. Particularly, variability is recorded for 2Φ and 1Φ classes for QF, whereas for feldspars of QFKa, the variability is observed for 4Φ and 5Φ classes. As for quartz, a tendency towards bimodality is recorded for feldspars particularly for samples TK8, TK20, TK41 and TK50 of fabric QF and for sample TK69 of fabric QFKa.

According to morphometric indices (Table 8), feldspars of both fabrics QF and QFKa may be defined as elongated with a weak tendency to circularity. Furthermore, grains are sub-angular and square shaped, as described by roundness and rectangularity values.

Alike quartz, it can be observed that a poorly sorted sediment characterises also feldspar distributions. Moreover, similar to quartz of fabric QF, these are very to positively skew distributed according to their coarse/medium-grained nature.

About morphometry, even if shape may be considered quite similar, feldspars are less circular and rounded and more elongated than quartz grains of both QF and QFKa.

Carbonate aggregates Carbonate aggregate grain-size distribution for fabric QFKa is negatively skewed,

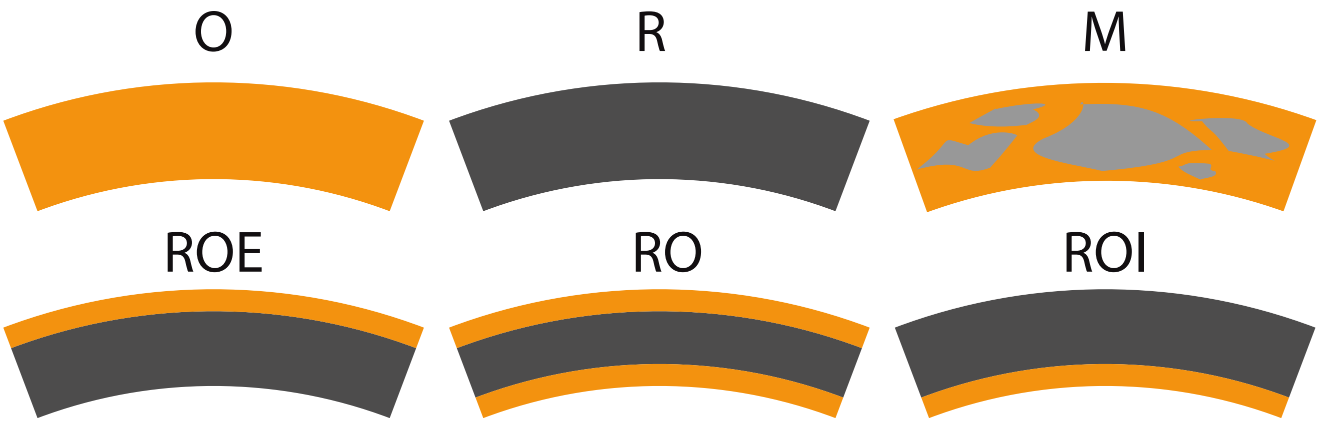

Fig. 4 Oxidation structures of the pottery fabric reported in Table 5. O, oxidised domains; R, reduced domains; M, marbled structure; E, external; I, internal. From left to right, acronyms report the oxidation sequence from the core to the surfaces

mesokurtic and poorly sorted according to the computed graphic statistical parameters with a prevalence of the 125–250 μm class (fine sand). Particularly, variability is recorded for 1Φ and 3Φ classes while the mean Mz value is 1.60Φ for sample TK69 and 2.32Φ for sample TK66. As previously observed for quartz and feldspars, grain-size distribution of sample TK69 shows a weak tendency to bimodality.

According to roundness and rectangularity values (Table 8), these inclusions are sub-angular grains with a quite squared shape. A weak tendency to circularity, which increased in the 6Φ class, and more to elongation are also observed.

XRF

The bulk chemical composition of the potsherds is essentially classifiable as Ca poor, except for TK2, TK3 and TK7 (Table 9). The prevalent oxides are SiO_2, Al_2O_3, Fe_2O_3 and K_2O, with more or less dispersed distribution of the data. Anomalous P_2O_5 concentrations were determined for the samples TK32 and TK33. The LOI ranges from 2.00 to 14.80 wt%.

SiO_2 is negatively correlated ($-0.1 < r < -0.7$) with the other oxides, whereas Al_2O_3 shows no correlation with Fe_2O_3 ($r = 0.04$) and moderate to strong positive correlation with Na_2O ($r = 0.35$), K_2O ($r = 0.65$) and Rb ($r = 0.80$). P_2O_5 shows clear correlation only with Sr ($r = 0.70$).

The two scatter plots in Fig. 6 essentially confirm the difference between the fabric groups Q* and QF* and add some details about the chemical groupings of ceramics. As a whole, the fabrics with Ka have lower MgO/CaO and those of group Q* have higher SiO_2/K_2O. The QKa samples can be divided at least into three subgroups and QF into two main subgroups. The scatter plot Rb vs. Zr (Fig. 6b) highlights a common chemical fingerprint for the Q* fabrics.

Raw materials

Petrography and mineralogy

The grain-size distribution of the sediments from the Takarkori swamp area was classified after Shepard's ternary diagram as 'sands' ($n = 13$), 'silty sands' ($n = 9$) and 'sandy silt' ($n = 1$) (Table 10). As shown in Table 11, quartz is the most abundant mineral in the analysed sediments, followed by illite-muscovite, kaolinite and chlorite. Feldspars occur in minor amounts. Exceptional quantities of calcite were detected in TKS10 and TKS12, whereas the only sample containing dolomite is TKS17. Traces of gypsum occur in samples from TKS18 to TKS22.

Under the optical microscope, the seven briquettes show three different fabrics, in analogy to pottery (Table 12). The first (Q) has monocrystalline quartz as framework grains and an iron-rich clay matrix, with more or less fine muscovite (Fig. 7a, b). In the second (QA), the additional presence of ARF was observed (Fig. 7c, d). Carbonate aggregates (Ka) in variable amounts are distinctive of the third fabric (QKa). Traces of feldspars were detected in thin section (Table 12).

XRF

Almost all the local sediments are Ca poor (CaO < 5 wt%), except for TKS10, TKS12 and TKS17 (Table 13). As for the composition of the potsherds, SiO_2, Al_2O_3 and Fe_2O_3 are prevalent, with less dispersed distribution of the data. The

Fig. 5 Thin section overview and fabric of the ceramics. **a** Fabric Q (TK14, 2.5×, P). **b** Fabric Q (TK14, 2.5×, XP). **c** Fabric QA (TK27, 2.5×, P). **d** Fabric QVe (TK06, 2.5×, P). **e** Fabric QF (TK32, 2.5×, P). **f** Fabric QF (TK60, 2.5×, XP). **g** Fabric QKa (TK02, 2.5×, XP). **h** Fabric QFKa (TK69, 2.5×, XP). Qz, quartz; Ka, carbonate aggregate; Ia, ferruginous aggregate; ARF, argillaceous rock fragment; Pl, plagioclase; Kfs, K-feldspar; Bt, biotite ▶

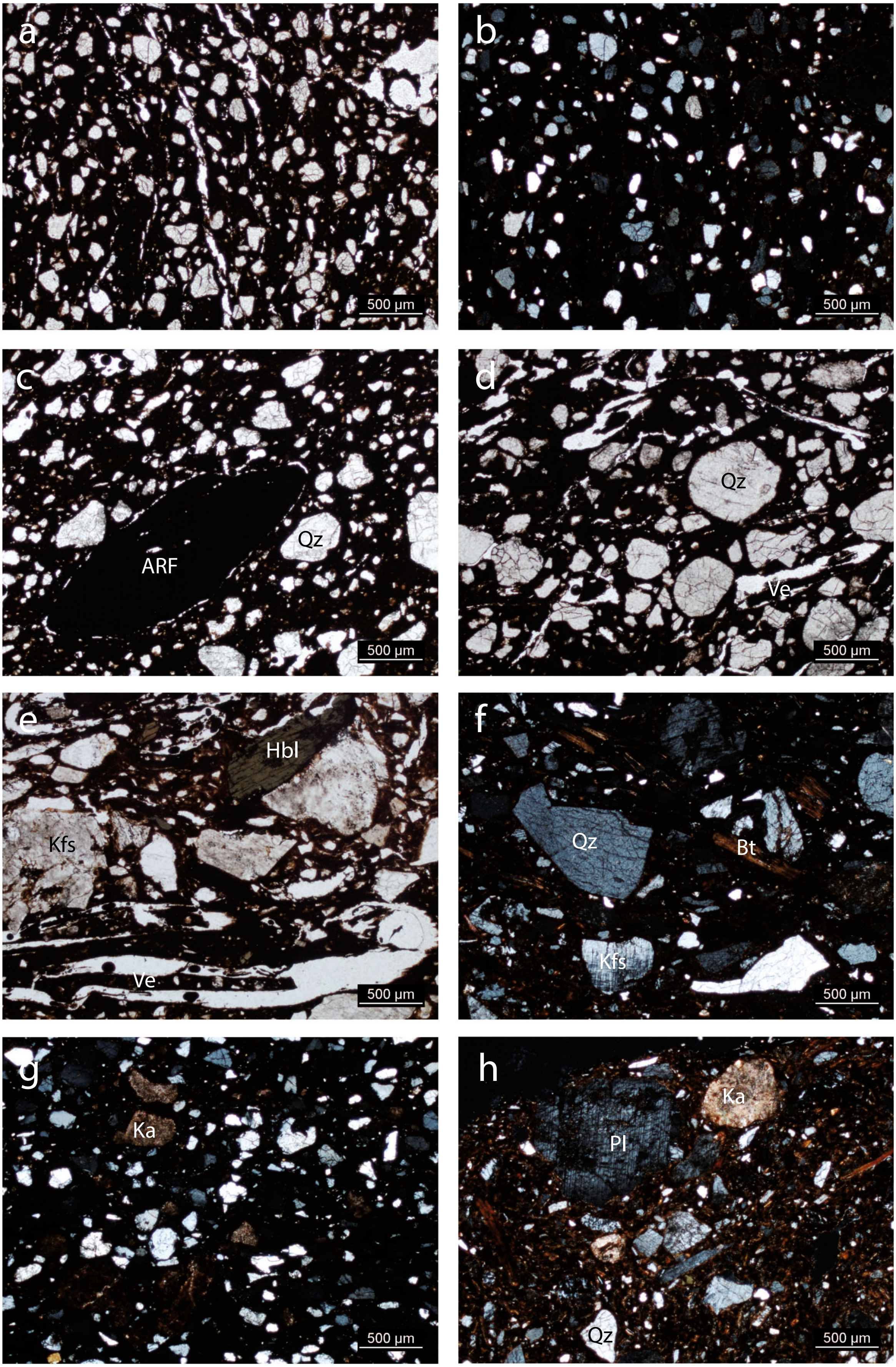
a
500 µm
b
500 µm
c
ARF
Qz
500 µm
d
Qz
Ve
500 µm
e
Hbl
Kfs
Ve
500 µm
f
Qz
Bt
Kfs
500 µm
g
Ka
500 µm
h
Ka
Pl
Qz
500 µm

Table 6 Volume percentages of non-plastic inclusions (NPIs) obtained by ImageJ

Samples	NPIs			16–32 μm (6Φ)			32–63 μm (5Φ)			63–125 μm (4Φ)			125–250 μm (3Φ)			250–500 μm (2Φ)			> 500 μm (1Φ)		
	Qz	Fsp	Ka	Qz	Fsp	Ka	Qz	Fsp	Ka	Qz	Fsp	Ka	Qz	Fsp	Ka	Qz	Fsp	Ka	Qz	Fsp	Ka
Fabric QF																					
TK08	15.21	6.59	–	7.24	1.40	–	21.49	9.99	–	29.39	27.27	–	24.49	29.28	–	17.39	32.06	–	0.00	0.00	–
TK12	11.88	9.38	–	1.06	0.15	–	7.53	1.52	–	30.55	9.16	–	25.45	28.46	–	28.61	36.59	–	6.80	24.12	–
TK20	9.01	12.84	–	13.86	1.41	–	28.27	6.02	–	20.64	16.82	–	27.69	27.08	–	9.54	48.67	–	0.00	0.00	–
TK21	7.15	3.79	–	0.81	0.06	–	3.97	0.29	–	13.47	4.38	–	22.62	12.94	–	25.11	48.68	–	34.02	33.64	–
TK23	7.01	6.05	–	1.23	0.04	–	5.00	0.49	–	17.79	2.63	–	17.94	12.80	–	18.29	22.13	–	39.75	61.91	–
TK28	10.92	7.24	–	1.22	0.28	–	5.31	1.50	–	15.20	6.64	–	19.86	14.14	–	38.45	26.69	–	19.95	50.75	–
TK31	11.95	6.27	–	0.99	0.09	–	4.36	0.27	–	11.81	2.38	–	15.68	10.54	–	19.37	26.66	–	47.78	60.06	–
TK32	12.97	7.43	–	0.76	0.05	–	3.84	0.42	–	12.92	3.59	–	20.69	10.47	–	20.32	32.02	–	41.46	53.45	–
TK33	8.67	4.49	–	0.90	0.14	–	4.35	0.90	–	12.00	8.77	–	18.08	20.46	–	24.83	29.01	–	39.84	40.73	–
TK35	5.75	14.43	–	9.22	1.33	–	23.28	4.09	–	22.90	11.37	–	23.58	19.64	–	21.03	46.67	–	0.00	16.91	–
TK36	11.76	6.88	–	0.32	0.06	–	2.24	0.38	–	8.80	4.04	–	12.28	8.78	–	12.99	35.77	–	63.38	50.97	–
TK41	8.23	13.11	–	5.55	0.31	–	11.66	2.41	–	18.32	12.16	–	64.48	16.18	–	0.00	38.62	–	0.00	30.32	–
TK42	10.96	8.97	–	0.80	0.11	–	3.76	0.31	–	9.44	2.18	–	19.79	8.36	–	26.07	29.56	–	40.14	59.48	–
TK44	6.16	12.32	–	12.00	6.85	–	29.77	7.05	–	34.09	17.35	–	24.14	1.86	–	0.00	25.48	–	0.00	41.41	–
TK45	7.75	5.02	–	0.94	0.25	–	6.78	1.05	–	27.34	6.58	–	21.84	13.26	–	23.13	14.62	–	19.98	64.24	–
TK46	7.86	8.31	–	0.60	0.08	–	3.52	0.31	–	12.72	3.34	–	20.16	9.25	–	28.32	14.48	–	34.68	72.53	–
TK47	6.79	6.76	–	0.68	0.07	–	4.17	0.24	–	17.77	3.64	–	12.88	17.81	–	22.31	29.00	–	42.20	49.24	–
TK48	5.53	8.31	–	1.77	0.22	–	10.17	0.98	–	20.48	5.21	–	22.42	19.41	–	13.40	21.44	–	31.76	52.74	–
TK49	7.58	14.75	–	4.82	1.10	–	8.21	4.68	–	9.20	13.70	–	38.52	28.64	–	39.26	44.03	–	0.00	7.85	–
TK50	7.10	9.85	–	7.04	2.78	–	21.54	6.20	–	29.00	13.99	–	17.20	20.98	–	25.23	40.78	–	0.00	15.26	–
TK58	7.35	11.13	–	1.25	0.14	–	5.95	1.17	–	13.89	5.10	–	24.00	14.04	–	38.46	31.12	–	16.44	48.42	–
TK59	14.53	5.61	–	0.21	0.24	–	1.36	0.68	–	5.35	2.82	–	6.93	8.43	–	6.16	35.30	–	79.98	52.53	–
TK60	6.63	8.36	–	1.52	0.19	–	5.45	0.19	–	19.59	1.57	–	25.66	9.39	–	25.76	37.18	–	22.02	51.48	–
TK61	11.30	7.97	–	0.33	0.14	–	2.50	0.95	–	8.20	4.33	–	10.23	10.78	–	15.72	32.15	–	63.01	51.65	–
TK62	10.17	8.89	–	0.42	0.06	–	2.83	0.32	–	10.86	5.02	–	13.00	19.10	–	21.72	31.87	–	51.17	43.62	–
TK63	8.82	8.67	–	0.45	0.02	–	2.84	0.24	–	11.81	2.38	–	17.13	15.43	–	15.37	30.91	–	52.39	51.03	–
TK64	6.29	4.64	–	1.10	0.02	–	6.16	0.91	–	20.65	5.70	–	19.15	26.79	–	9.51	33.84	–	43.44	32.75	–
TK65	3.42	2.94	–	1.41	0.27	–	8.80	0.58	–	31.31	3.57	–	37.88	17.33	–	6.24	16.15	–	14.36	62.10	–
TK67	7.41	8.83	–	0.58	0.22	–	2.08	0.41	–	6.21	3.18	–	13.91	11.62	–	19.47	23.88	–	57.74	60.69	–
TK68	4.78	2.47	–	1.70	0.94	–	6.52	1.57	–	13.58	5.77	–	19.30	22.22	–	37.48	30.81	–	21.43	38.70	–
Fabric QFKa																					
TK66	9.33	4.43	1.18	1.34	1.06	0.00	7.53	4.35	2.04	20.84	13.82	9.93	26.92	26.96	62.18	22.83	34.68	25.85	20.54	19.12	0.00
TK69	9.11	9.00	4.11	1.56	9.53	4.57	5.92	22.84	5.92	5.12	20.21	3.69	25.25	22.78	28.51	46.03	24.64	13.98	16.12	0.00	43.32

Normalised grain-size distributions for NPIs

Table 7 Statistical parameters for quartz, feldspars and carbonate aggregates inclusions of the analysed samples (phi units)

	Graphic method[a]															Moment method[b]											
	Md			Mz			σ_1			Sk_1			K_G			x_m			σ_2			α_3			K_4		
	Qz	Fsp	Ka	Qz	Fsp	Ka	Qz	Fsp	Ka	Qz	Fsp	Ka	Qz	Fsp	Ka	Qz	Fsp	Ka	Qz	Fsp	Ka	Qztz	Fsp	Ka	Qz	Fsp	Ka
Fabric QF																											
TK08	3.28	2.61	–	3.26	2.65	–	1.57	1.11	–	0.16	0.11	–	1.31	0.83	–	3.27	2.69	–	1.39	1.08	–	0.09	0.44	–	2.11	2.31	–
TK12	2.54	1.71	–	2.53	1.73	–	1.35	1.06	–	0.02	0.08	–	0.92	0.95	–	2.57	1.78	–	1.26	0.98	–	0.08	0.46	–	2.33	2.79	–
TK20	3.62	2.05	–	3.59	2.29	–	1.30	1.04	–	−0.03	0.38	–	0.82	0.93	–	3.59	2.34	–	1.49	1.00	–	−0.03	1.02	–	1.92	3.26	–
TK21	1.64	1.34	–	1.76	1.31	–	1.26	0.84	–	0.18	0.06	–	0.80	1.04	–	1.81	1.39	–	1.50	0.67	–	0.63	0.88	–	2.56	3.88	–
TK23	1.56	0.81	–	1.80	1.02	–	1.39	0.86	–	0.27	0.42	–	0.73	0.96	–	1.84	1.08	–	1.82	0.72	–	0.59	1.41	–	2.23	4.42	–
TK28	1.78	0.98	–	1.99	1.25	–	1.26	1.05	–	0.24	0.43	–	1.05	0.98	–	2.01	1.32	–	1.42	1.06	–	0.66	1.20	–	2.82	3.88	–
TK31	1.11	0.83	–	1.51	1.00	–	1.30	0.82	–	0.46	0.38	–	0.82	0.97	–	1.59	1.06	–	1.65	0.65	–	0.95	1.45	–	2.87	4.93	–
TK32	1.42	0.93	–	1.64	1.06	–	1.27	0.84	–	0.28	0.32	–	0.83	0.96	–	1.70	1.16	–	1.57	0.71	–	0.72	1.29	–	2.55	4.40	–
TK33	1.41	1.32	–	1.64	1.47	–	1.27	1.10	–	0.30	0.25	–	0.83	0.85	–	1.69	1.51	–	1.56	1.07	–	0.82	0.74	–	2.79	2.71	–
TK35	3.24	1.71	–	3.24	1.91	–	1.38	1.11	–	0.02	0.27	–	0.80	1.10	–	3.26	1.93	–	1.62	1.22	–	0.11	0.93	–	1.89	3.64	–
TK36	0.79	0.98	–	1.22	1.07	–	1.14	0.83	–	0.58	0.27	–	0.99	0.99	–	1.25	1.17	–	1.30	0.70	–	1.36	1.31	–	3.78	4.65	–
TK41	2.78	1.51	–	3.04	1.63	–	0.92	1.17	–	0.48	0.21	–	1.05	0.97	–	3.08	1.69	–	0.81	1.18	–	1.38	0.79	–	3.73	2.97	–
TK42	1.38	0.84	–	1.56	0.98	–	1.21	0.79	–	0.28	0.35	–	0.86	0.98	–	1.63	1.05	–	1.43	0.60	–	0.89	1.56	–	3.08	5.71	–
TK44	3.76	1.34	–	3.76	1.87	–	1.06	1.65	–	0.04	0.49	–	0.90	0.76	–	3.80	1.94	–	0.93	2.67	–	0.18	0.85	–	2.04	2.38	–
TK45	2.31	0.78	–	2.27	1.14	–	1.35	1.04	–	−0.02	0.54	–	0.79	1.02	–	2.31	1.16	–	1.62	1.06	–	0.09	1.44	–	2.02	4.18	–
TK46	1.52	0.69	–	1.68	0.90	–	1.23	0.82	–	0.23	0.48	–	0.82	1.38	–	1.74	0.95	–	1.41	0.69	–	0.70	1.90	–	2.68	6.04	–
TK47	1.35	1.03	–	1.70	1.22	–	1.33	0.93	–	0.36	0.32	–	0.71	0.84	–	1.71	1.27	–	1.70	0.79	–	0.72	0.92	–	2.31	3.11	–
TK48	2.22	0.95	–	2.17	1.25	–	1.51	1.03	–	0.02	0.44	–	0.72	0.83	–	2.19	1.31	–	2.08	1.02	–	0.26	1.05	–	1.90	3.40	–
TK49	2.28	1.96	–	2.46	2.13	–	1.15	1.05	–	0.32	0.25	–	1.22	1.02	–	2.51	2.17	–	1.25	1.07	–	1.17	0.77	–	3.63	3.41	–
TK50	3.26	1.85	–	3.16	2.12	–	1.36	1.27	–	−0.06	0.31	–	0.77	1.06	–	3.18	2.13	–	1.58	1.52	–	0.07	0.79	–	1.91	3.09	–
TK58	1.87	1.05	–	2.07	1.23	–	1.22	0.98	–	0.24	0.34	–	−1.57	0.98	–	2.08	1.30	–	1.36	0.92	–	0.65	1.17	–	2.92	3.99	–
TK59	0.63	0.95	–	0.83	1.05	–	0.86	0.81	–	0.53	0.28	–	2.15	0.97	–	0.93	1.15	–	0.91	0.70	–	2.26	1.56	–	7.20	6.14	–
TK60	2.09	0.97	–	2.12	1.05	–	1.33	0.78	–	0.07	0.24	–	0.86	0.93	–	2.15	1.12	–	1.57	0.58	–	0.36	1.33	–	2.40	5.59	–
TK61	0.79	0.97	–	1.18	1.10	–	1.12	0.88	–	0.57	0.32	–	1.10	0.98	–	1.22	1.21	–	1.26	0.82	–	1.47	1.37	–	4.16	4.73	–
TK62	0.98	1.20	–	1.38	1.34	–	1.20	0.97	–	0.50	0.23	–	0.92	0.86	–	1.44	1.37	–	1.39	0.85	–	1.08	0.80	–	3.17	2.90	–
TK63	0.95	0.98	–	1.40	1.14	–	1.23	0.87	–	0.53	0.31	–	0.79	0.87	–	1.49	1.20	–	1.50	0.69	–	0.93	0.97	–	2.74	3.28	–
TK64	1.69	1.51	–	1.88	1.55	–	1.45	1.01	–	0.22	0.09	–	0.68	0.83	–	1.90	1.58	–	2.02	0.90	–	0.45	0.50	–	1.89	2.59	–
TK65	2.77	0.81	–	2.61	1.13	–	1.28	0.96	–	−0.16	0.48	–	1.28	0.85	–	2.68	1.15	–	1.40	0.91	–	−0.35	1.33	–	2.75	4.17	–
TK67	0.87	0.82	–	1.21	1.02	–	1.09	0.86	–	0.51	0.41	–	0.99	0.97	–	1.27	1.09	–	1.19	0.76	–	1.40	1.52	–	4.34	5.19	–
TK68	1.76	1.37	–	1.98	1.48	–	1.32	1.08	–	0.27	0.21	–	1.00	0.88	–	2.01	1.54	–	1.55	1.13	–	0.73	1.00	–	2.86	3.94	–

Table 7 (continued)

	Graphic method[a]														
	Md			Mz			σ_1			Sk_1			K_G		
	Qz	Fsp	Ka	Qz	Fsp	Ka	Qz	Fsp	Ka	Qz	Fsp	Ka	Qz	Fsp	Ka
Fabric QFKa															
TK66	2.25	1.89	2.39	2.23	1.99	2.32	1.37	1.18	0.71	0.02	0.14	−0.06	0.86	0.97	1.25
TK69	1.74	3.13	1.48	1.87	3.17	1.60	1.04	1.42	1.37	0.32	0.07	0.29	1.16	0.76	0.97

	Moment method[b]											
	x_m			σ_2			α_3			K_4		
	Qz	Fsp	Ka	Qz	Fsp	Ka	Qztz	Fsp	Ka	Qz	Fsp	Ka
Fabric QFKa												
TK66	2.26	2.03	2.38	1.62	1.30	0.43	0.23	0.57	0.57	2.25	2.92	3.99
TK69	1.93	3.20	1.79	1.21	1.73	2.05	1.08	0.17	0.99	4.16	1.81	3.21

[a] Symbols for the graphic method: Md = median; Mz = mean; σ_1 = sorting; Sk_1 = skewness; K_G = kurtosis

[b] Symbols for the moment method: x_m = mean; σ_2 = sorting; α_3 = skewness; K_4 = kurtosis

LOI ranges from 0.85 to 18.15 wt%, with strong negative correlation with SiO_2. Other than the moderate to strong negative correlation between SiO_2 and the other oxides, Al_2O_3 shows strong positive correlation with Fe_2O_3 ($r = 0.86$), Na_2O ($r = 0.76$) and K_2O ($r = 0.94$). P_2O_5 shows the highest positive correlation with Sr ($r = 0.69$), Fe_2O_3 ($r = 0.68$) and TiO_2 ($r = 0.63$).

A selection of elements and oxides is shown in Figs. 6b and 8 and plotted according to the sediment types. Two groups of sands are distinguishable. The sediments from the northern side of Tadrart Acacus (Wadi Tanezzuft) show higher concentrations of Fe_2O_3 and Rb and lower SiO_2/Al_2O_3 values, compared to those of Takarkori (Fig. 1d, e).

Discussion

Fabric variability in times

The pottery fabric analysis, integrated with the mineralogical study (XRPD), provided a semi-quantitative dataset useful to distinguish two fabric groups according to the absence/presence of the plutonic NPIs (Q* and QF*). The relative amounts of secondary NPIs affected the classification in subgroups of fabric. Even though sometimes their abundance is not enough to provide a clear classification, the occurrence of a given NPI highlights differences on the petrofacies useful to identify the sedimentary environment of the raw materials.

The grain-size distributions of QF and QFKa (for quartz, feldspars and carbonate aggregates) show a broad tendency to bimodality as previously observed also for five samples of fabric QKa. There, it was interpreted as the simultaneous occurrence of the finer fraction due to some erosion and deposition of the soft carbonate aggregates. Together with the textural features of quartz inclusions, this indicates a sedimentary facies in a lacustrine depositional environment, where the change of water content in the sediment led to calcite precipitation (Eramo et al. 2014). This seems to be confirmed in the graph median (Md) vs. interquartile (Qda) of the grain-size distribution of quartz grains in the different fabrics (Fig. 9), where the samples with Ka are classified between flowing and quiet water. Moreover, the low percentage of carbonate aggregates computed also for QFKa which is quite the same for QKa confirms the accidental nature of these inclusions; i.e. no deliberate addition for both fabrics can be suggested. Bimodality for feldspars and, particularly, for quartz of QF has to be verified, considering that, on the one hand, the mean volume percentage of these inclusions is consistent with the definition of tempering and that grains are more angular. But on the other hand, these values are too similar to represent a deliberate addition, as seen also for Q and QKa. Moreover, fluviatile sediment may be characterised by more angular grains due to their textural immaturity.

Table 8 Median values of morphometric indexes for quartz and calcareous aggregates (overall datum, phi units)

	Groups	16–32 μm (6Φ)	32–63 μm (5Φ)	63–125 μm (4Φ)	125–250 μm (3Φ)	250–500 μm (2Φ)	> 500 μm (1Φ)
Circularity							
Qz	QF	0.76	0.68	0.61	0.50	0.44	0.37
	QFKa	0.74	0.69	0.61	0.51	0.45	0.53
Fsp	QF	0.71	0.61	0.53	0.45	0.37	0.33
	QFKa	0.66	0.57	0.51	0.42	0.41	0.33
Ka	QFKa	0.63	0.46	0.52	0.50	0.44	0.45
Aspect ratio							
Qz	QF	1.56	1.65	1.70	1.87	1.81	1.84
	QFKa	1.53	1.62	1.78	1.76	1.84	1.48
Fsp	QF	1.66	1.75	1.80	1.86	1.94	1.89
	QFKa	1.73	1.76	1.79	1.93	1.90	2.34
Ka	QFKa	1.80	1.88	1.63	1.66	2.00	1.99
Roundness							
Qz	QF	0.64	0.61	0.59	0.54	0.55	0.54
	QFKa	0.65	0.62	0.56	0.57	0.55	0.68
Fsp	QF	0.60	0.57	0.55	0.54	0.52	0.53
	QFKa	0.58	0.57	0.56	0.52	0.53	0.45
Ka	QFKa	0.55	0.53	0.61	0.60	0.50	0.50
Rectangularity							
Qz	QF	0.53	0.50	0.49	0.45	0.46	0.45
	QFKa	0.53	0.51	0.47	0.43	0.50	0.62
Fsp	QF	0.52	0.48	0.46	0.43	0.42	0.42
	QFKa	0.48	0.45	0.42	0.40	0.47	0.53
Ka	QFKa	0.45	0.40	0.56	0.53	0.41	0.36

As compared to carbonate aggregates of fabric QKa (Eramo et al. 2014), grain-size distributions for fabric QFKa confirmed a tendency to bimodality and to poor sorting. The overall volume percentage of carbonate aggregates is quite the same for both fabrics, that is 1.67% for QFKa and 1.76% for QKa. Both distributions are mesokurtic, but while that of QKa is very positively skewed, fabric QFKa is negatively skewed. The low number of samples belonging to fabric QFKa must be always considered. Eventually, morphometry is very similar for both fabrics, although grains of fabric QFKa were less rounded and more elongated when compared with those of QKa according to morphometric parameters of feldspars of the same fabric.

The coarser grain size of fabric QF compared with the other five fabrics may strengthen the hypothesis of a proximal/non-local source for this fabric. In Fig. 9, it can be observed that QF samples are distributed in different clusters, showing possible different provenances, as also evidenced by the chemical composition (Fig. 6).

Comparing the results obtained with texture and morphometry of quartz for fabrics Q and QKa (Eramo et al. 2014), it can be observed that a poorly sorted sediment characterises all the studied fabrics.

However, fabric QF is coarse grained while the other fabrics are finer grained. Actually, its grain-size distribution is positively skewed while those of Q, QVe, QA, QKa and QFKa are all symmetrical. Similarly, according to their higher variability, distributions of fabrics QF and QFKa are platykurtic in respect of the mesokurtic distributions of both Q and QKa. Moreover, the coarser grain size of fabric QF may confirm the hypothesis of a possible sub-local source closer to Takarkori rock shelter for sample TK43 of fabric Q, characterised by a coarse/medium sand distribution too, beside the evidently non-local pottery represented by QF in the same area (Eramo et al. 2014).

Finally, quartz for both fabrics QF and QFKa are less circular and more elongated than those of fabrics Q and QKa. These inclusions for all the fabrics may be described between sub-angular and sub-rounded, even if those of QF and QFKa are less rounded. Particularly, quartz grains of fabric QF were the least circular and rounded and the most elongated. However, quartz grains of all the fabrics show a quite angular shape.

Table 9 Bulk chemical composition of ceramics determined by XRF

Sample	SiO_2	TiO_2	Al_2O_3	Fe_2O_3	MnO	MgO	CaO	Na_2O	K_2O	P_2O_5	LOI	Rb	Sr	Y	Zr	Nb
TK01	60.89	1.16	15.91	14.53	0.09	2.17	2.64	0.43	2.78	0.29	6.07	71	215	28	196	20
TK02	61.77	1.09	11.19	6.94	0.16	1.32	13.79	0.67	2.47	0.23	10.19	37	128	20	191	13
TK03	60.34	1.05	11.52	6.27	0.13	1.55	14.17	0.73	3.23	0.34	11.45	31	90	15	132	9
TK04	67.67	1.34	15.93	10.72	0.09	1.08	0.58	0.22	1.64	0.12	8.03	55	89	25	300	22
TK05	73.21	1.06	15.46	5.55	0.04	0.98	0.63	0.33	2.47	0.27	5.86	45	74	16	145	12
TK06	72.72	0.87	14.17	4.89	0.02	1.01	0.69	0.42	4.55	0.31	2.00	49	73	15	155	11
TK07	62.76	1.12	11.99	7.16	0.13	1.36	12.04	0.35	2.24	0.15	9.23	42	150	25	242	17
TK08	69.08	0.89	17.79	5.40	0.08	1.16	1.16	0.68	4.12	0.17	9.52	56	46	14	93	7
TK09	67.19	0.88	16.42	6.12	0.07	2.19	2.36	0.65	3.76	0.33	9.52	57	111	17	182	11
TK10	64.70	1.54	19.42	7.82	0.08	1.42	2.18	0.30	2.02	0.95	8.73	50	192	23	174	17
TK11	72.62	1.18	15.58	5.52	0.08	1.07	1.00	0.23	1.77	0.33	8.47	38	83	15	161	11
TK12	62.86	0.86	21.73	6.33	0.05	1.25	1.12	0.95	4.78	0.14	7.20	127	89	28	238	16
TK13	71.92	0.83	15.33	4.86	0.04	1.31	1.48	0.27	4.02	0.18	6.95	56	107	21	252	15
TK14	71.25	0.99	17.98	5.79	0.09	1.16	1.06	0.23	1.98	0.17	7.81	69	104	20	200	16
TK15	70.18	0.98	17.59	5.50	0.08	1.16	1.19	0.22	2.04	0.19	9.19	59	85	18	144	13
TK16	67.00	1.01	17.25	5.95	0.07	2.00	1.71	0.67	4.87	0.28	7.62	72	111	20	208	15
TK17	73.50	0.84	15.48	5.37	0.09	1.29	1.44	0.30	2.36	0.13	7.30	54	93	19	210	14
TK18	75.39	0.85	13.11	5.32	0.07	1.30	2.29	0.19	2.18	0.13	4.08	38	66	14	163	11
TK19	74.80	0.81	12.26	5.18	0.07	1.28	2.68	0.28	3.28	0.14	5.29	47	91	17	196	13
TK20	57.17	0.74	19.58	5.88	0.07	1.89	2.70	1.67	9.01	0.65	5.86	92	176	22	244	12
TK21	58.41	0.86	24.31	7.50	0.11	1.19	1.10	0.60	6.42	0.21	11.00	128	98	39	320	18
TK22	73.84	0.71	13.03	4.51	0.03	1.61	3.08	0.27	3.00	0.16	9.78	53	82	15	211	11
TK23	59.35	0.88	25.59	6.45	0.06	1.04	1.09	0.51	4.81	0.18	13.43	121	122	24	261	19
TK24	75.83	0.77	13.01	4.42	0.05	1.08	0.81	0.40	3.47	0.18	5.28	57	72	16	164	11
TK25	73.91	0.79	13.17	4.82	0.04	1.53	2.49	0.31	3.49	0.21	7.67	51	81	15	201	10
TK26	77.73	0.81	13.50	4.66	0.07	0.91	0.72	0.24	1.83	0.12	8.06	60	80	19	192	13
TK27	70.67	0.85	14.46	4.66	0.09	1.08	0.77	0.84	6.09	0.24	7.02	61	92	18	196	14
TK28	61.79	0.96	18.39	6.50	0.06	1.84	2.54	1.62	5.02	0.51	8.21	105	154	33	274	17
TK29	67.69	1.05	14.42	7.20	0.11	1.80	4.69	0.44	2.90	0.33	8.30	54	181	23	183	18
TK30	69.59	1.15	13.26	7.54	0.06	1.56	3.81	0.28	2.73	0.48	11.75	37	122	22	219	16
TK31	58.92	0.76	24.69	6.57	0.05	0.90	1.32	0.55	5.57	0.18	14.80	112	63	25	177	15
TK32	58.56	0.85	19.74	7.26	0.09	0.70	1.77	1.31	4.55	5.61	6.59	82	317	24	282	13
TK33	56.23	0.83	22.19	7.44	0.07	1.11	1.70	1.13	5.93	3.56	9.39	105	262	32	267	16
TK34	63.07	1.40	19.42	6.60	0.04	1.48	2.25	0.42	5.20	0.67	8.87	66	123	25	182	19
TK35	59.47	0.79	22.87	6.44	0.04	0.97	1.95	0.48	6.84	0.34	8.40	121	99	18	135	12
TK36	62.21	0.77	21.41	5.79	0.04	1.10	0.86	0.51	7.77	0.15	8.02	144	77	21	167	14
TK37	69.22	1.01	17.64	6.42	0.06	1.61	1.61	0.22	2.82	0.14	11.09	67	73	17	151	13
TK38	74.93	0.80	14.99	4.12	0.04	1.12	1.32	0.30	2.45	0.18	8.67	44	68	13	164	9
TK39	71.36	1.04	14.74	5.08	0.03	1.16	1.56	0.30	3.60	0.64	4.47	45	95	17	158	14
TK40	70.41	0.85	15.41	5.65	0.05	1.85	3.07	0.37	3.17	0.17	6.09	49	78	13	166	10
TK41	64.28	0.56	21.65	3.92	0.03	0.96	1.54	0.91	5.12	0.77	7.48	119	134	14	136	11
TK42	67.62	0.53	21.74	3.76	0.03	0.86	0.95	0.79	4.45	0.12	7.38	92	56	9	95	7
TK43	67.93	0.87	16.30	7.06	0.13	2.07	0.90	0.29	4.86	0.20	8.52	106	94	16	100	11
TK44	64.46	0.82	16.47	6.24	0.12	1.59	2.80	1.95	5.69	0.35	5.63	62	179	13	129	8
TK45	63.42	1.10	16.37	7.61	0.20	2.75	2.66	1.41	5.00	0.22	9.05	97	185	21	136	15
TK46	61.09	0.89	23.24	6.95	0.06	1.19	1.28	0.67	4.85	0.13	10.08	109	68	21	139	11
TK47	56.14	0.99	22.96	6.96	0.06	1.54	2.20	1.10	7.65	0.64	11.07	127	133	24	247	20
TK48	61.06	0.68	21.21	5.63	0.04	1.03	1.78	0.99	6.94	0.40	4.99	144	141	27	214	16
TK49	60.10	0.59	21.21	5.74	0.06	0.86	0.78	0.59	8.95	0.14	11.19	161	60	29	266	17

Table 9 (continued)

Sample	SiO_2	TiO_2	Al_2O_3	Fe_2O_3	MnO	MgO	CaO	Na_2O	K_2O	P_2O_5	LOI	Rb	Sr	Y	Zr	Nb
TK50	54.82	1.04	23.90	7.28	0.06	1.64	2.68	0.58	8.11	0.31	11.31	131	128	30	251	21
TK51	72.41	0.92	14.22	5.72	0.06	1.44	1.85	0.32	3.04	0.13	6.17	49	70	17	180	13
TK52	70.16	1.17	16.31	6.15	0.09	1.50	1.04	0.30	2.77	0.68	7.44	58	93	23	220	18
TK53	68.99	0.96	15.57	10.85	0.05	0.77	1.97	0.13	1.01	0.21	5.30	31	72	24	547	17
TK54	72.07	0.82	14.77	5.09	0.05	1.60	2.00	0.25	2.53	0.25	7.19	66	104	17	185	13
TK55	79.23	0.74	12.34	4.10	0.04	0.98	0.62	0.17	1.57	0.13	4.90	57	95	17	193	13
TK56	68.45	0.94	15.39	10.62	0.05	0.76	2.03	0.13	0.94	0.18	5.95	35	80	27	631	19
TK57	76.22	1.00	12.54	5.11	0.06	1.11	0.98	0.23	3.10	0.34	6.55	49	94	20	286	16
TK58	64.76	0.43	20.44	4.10	0.03	0.84	1.51	0.70	7.28	0.18	5.32	134	68	20	101	13
TK59	62.91	0.79	20.01	5.71	0.05	0.89	2.45	0.94	6.30	0.22	7.59	138	153	30	226	17
TK60	61.24	0.98	20.77	6.72	0.12	1.56	1.23	0.93	6.09	0.14	7.07	192	104	35	203	17
TK61	60.83	0.71	18.63	5.07	0.04	1.62	1.70	0.98	8.57	0.90	5.58	139	124	17	180	13
TK62	64.07	0.78	21.29	5.34	0.04	0.93	0.57	0.25	6.05	0.08	8.26	173	76	25	214	18
TK63	65.08	0.80	21.43	5.39	0.04	0.87	0.46	0.23	5.54	0.05	5.84	180	75	25	236	19
TK64	59.65	0.99	23.74	7.04	0.06	0.82	1.09	0.41	5.98	0.11	10.16	152	153	34	233	21
TK65	60.64	1.08	15.89	7.56	0.17	2.39	2.20	0.84	8.84	0.38	6.41	118	182	25	154	20
TK66	60.68	0.99	18.71	6.17	0.06	1.76	4.02	2.06	4.52	0.11	6.86	104	151	31	237	16
TK67	64.07	0.44	21.53	3.79	0.02	0.90	1.53	2.04	6.10	0.24	8.26	174	81	20	146	20
TK68	62.04	1.03	19.15	6.49	0.08	1.78	3.21	1.64	4.65	0.10	8.84	112	136	36	246	17
TK69	62.77	0.70	21.59	5.43	0.05	0.96	1.35	0.89	6.73	0.26	7.01	145	93	34	154	15

Concentrations of major and minor oxides and the LOI are expressed in wt% and of trace elements in mg/kg

The poor sorting may confirm the origin by a common fluviatile sediment with a greater or smaller aeolian component interpreted in terms of sedimentary facies in a wadi/swamp transition environment (i.e. flowing/quiet water) in a climatic transition from arid to wet conditions supposed previously for Q and QKa (Eramo et al. 2014).

The bulk chemical (Fig. 12) and mineralogical (Fig. 11) compositions of local sediments are more closely related to one another compared to those of potsherds. In the first case, they essentially mirror the more or less important component of quartz sand and carbonates in the sediment. In the second case, the presence of pottery fabrics characterised by feldspars and mafic

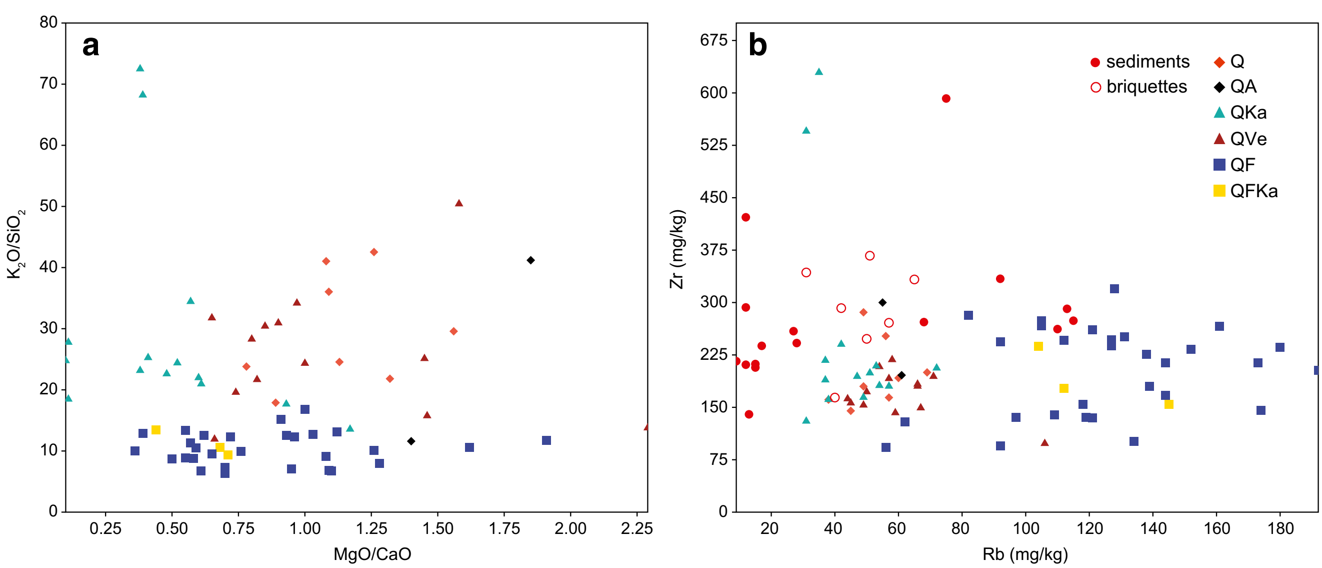

Fig. 6 **a** Scatter plot of oxide ratios of the pottery samples. **b** Scatter plot of Rb vs. Zr of the analysed pottery and sediments. Hollow symbols indicate the sediments used for the briquettes

minerals introduced more complexity in the dataset and less obvious general trends. The petrographical and chemical compatibility of some of the sandy silt sediments sampled in the area of Takarkori rock shelter shows that it was possible to obtain Q* fabrics from unprocessed local sediments. The photomicrographs of the selected sediments of local origin show that the fabrics Q, QA and QKa match with samples TKS05 (Fig. 7f), TKS02 (Fig. 7c, d), TKS04 (Fig. 7e) and TKS10 (Fig. 7g), and further demonstrate the natural availability of such petrofacies, without significant compositional/textural modifications (see below). If the Q* fabrics are marked by the Palaeozoic sandstones and shales, the QF* fabrics cannot be obtained from the same formations and find only some chemical (Fig. 6b) and mineralogical (Table 11) correlation with the sediments from Wadi Tanezzuft (TKS17–22). The characteristic presence of hornblende and micas, other than frequent feldspars, in the QF* fabrics points to the Tassili n'Ajjer granitic bedrock (ca. 50 km west-southwest from Takarkori; Fig. 2) as a source of these minerals. Such composition can be found along the wadis belonging to the drainage basin of the southern Tassili. The depositional environments inferred by the grain size parameters of the pottery samples of QF* fabrics (Fig. 9) identify different groups of original clays associable to flowing and quiet water environments, both possible in the lowlands at the south-western margin to the Tassili n'Ajjer.

Table 10 Grain-size distribution of the local sediments

Sample	$f < 2$ µm	$f = 2$–63 µm	$f > 63$ µm	Type
TKS01	0.83	2.69	96.48	Sand
TKS02	5.38	13.69	80.93	Sand
TKS03	3.26	9.75	86.99	Sand
TKS04	4.19	21.51	74.3	Silty sand
TKS05	4.52	29.12	66.36	Silty sand
TKS06	1.2	2.16	96.64	Sand
TKS07	2.24	4.84	92.92	Sand
TKS08	0.93	2.09	96.98	Sand
TKS09	3.52	3.64	92.84	Sand
TKS10	6.23	28.64	65.13	Silty sand
TKS11	5.82	16.51	77.67	Silty sand
TKS12	7.33	33.56	59.11	Silty sand
TKS13	0.77	2.71	96.52	Sand
TKS14	2.7	3.41	93.89	Sand
TKS15a	6.53	50.2	43.27	Sandy silt
TKS15b	6.86	27.18	65.96	Silty sand
TKS15c	5.23	20.41	74.36	Silty sand
TKS17	0.83	2.69	96.48	Sand
TKS18	5.38	13.69	80.93	Sand
TKS19	3.26	9.75	86.99	Sand
TKS20	4.19	21.51	74.3	Silty sand
TKS21	4.52	29.12	66.36	Silty sand
TKS22	1.2	2.16	96.64	Sand

Classification after Shepard (1954)

Table 11 Semi-quantitative (wt%) mineralogical composition of the unprocessed sediments (XRPD)

Sample	Ill + Ms	Kln	Chl	Qz	Fsp	Cal	Dol	Gyp
TKS01	2	1	0	97	0	0	0	0
TKS02	8	8	2	82	0	0	0	0
TKS03	5	5	1	88	0	0	0	0
TKS04	12	8	4	72	2	3	0	0
TKS05	15	10	4	67	2	3	0	0
TKS06	1	1	0	97	0	0	0	0
TKS07	3	3	1	93	1	0	0	0
TKS08	1	1	0	97	0	0	0	0
TKS09	3	3	1	94	0	0	0	0
TKS10	17	11	7	54	1	11	0	0
TKS11	9	7	2	81	1	0	0	0
TKS12	15	12	4	19	0	50	0	0
TKS13	1	1	1	94	1	1	0	0
TKS14	3	1	1	95	0	0	0	0
TKS15a	27	17	6	47	2	0	0	0
TKS15b	17	11	5	62	3	3	0	0
TKS15c	13	8	3	72	1	2	0	0
TKS17	14	8	3	50	6	3	16	0
TKS18	22	12	7	47	10	0	0	2
TKS19	16	15	6	58	4	0	0	1
TKS20	30	15	5	40	7	0	0	3
TKS21	12	16	3	65	3	0	0	1
TKS22	21	25	4	47	2	0	0	1

Mineral abbreviations after Whitney and Evans (2010)

Sustainability of local pottery production

The comparison between the local sediments and the potsherds dominated by monocrystalline quartz and iron-rich clay (Q* fabrics) showed that pottery production at Takarkori was sustainable, since clay, water and fuel were available during all the occupational phases.

The four fabrics (Q, QA, QKa and QVe) have a higher content of NPIs (Eramo et al. 2014) compared to that of QF* fabrics (Table 6) and thus a presumed lower plasticity, as ascertained on the analysed local sediments to prepare the briquettes. Although the composition/texture of some of the local sediment is very similar to that of Q* fabrics (cfr. Figs. 5 and 7), the high presence of small fragments of carbonised vegetal relics in QVe potsherds suggests some addition during the preparation of the paste. Due to the sandy texture of the local sediments compatible with the fabric group Q*, the use

Table 12 Petrographic outline of the unprocessed clays

Sample	Fabric*	Matrix	Texture	Mode(s) (μm)	Qm	Qp	Pl	Kfs	Ms	ARF	Ka	Ia	Bioclasts	Ep
TKS02	QA	i	Bimodal	125–250; 1000–2000	4	1	0	0	1	1	0	1	0	0
TKS04	Q	i	Bimodal	125–250; 1000–2000	4	1	1	0	1	0	1	1	1	1
TKS05	Q	i	Unimodal	125–250	4	0	1	0	1	0	1	1	0	1
TKS10	QKa	i	Bimodal	125–250; 1000–2000	4	1	1	0	1	0	3	1	0	1
TKS12	QKa	k	Unimodal	125–250	3	0	0	0	1	0	3	1	0	1
TKS15a	Q	m	Unimodal	63–125	4	0	0	0	3	0	0	1	0	1
TKS15b	Q	m	Bimodal	125–250; 1000–2000	4	1	0	0	2	0	0	1	0	1

Abbreviations as in Table 5

*The term 'fabric' is used in analogy to pottery

of animal dung for the preparation of the paste is supposed to improve the plasticity (London 1981), and thus the vegetal residues observed in the fabric QVe could be part of the added dung. Vegetal inclusions are also present in pastes of Late Acacus age (Table 5) but constituted by coarser vegetal fibres, stems, chaff and so on, whose voids left after combustion are visible already in the macroscopic observation. The difference in size, as well as the frequency of their presence, demonstrates the different nature of vegetal fibres in QVe and in the other fabrics (Fig. 5d, e). The smaller size of the vegetal remains present in the faeces (Abbink 1999), and the fine organic matter dispersed in the matrix differs from simple vegetal inclusions.

Together with the fabric evidences, enrichment in P in the bulk chemical composition of the pottery is reported by several authors (Collomb and Maggetti 1996; Shahack-Gross 2011), mainly as Ca phosphates. Unfortunately, the extent of such P enrichments in archaeometric (van Doosselaere et al. 2014; Kulkova and Kulkov 2016) and experimental (London 1981; Skibo et al. 1989; Abbink 1999; Tsetlin 2003) studies was not reported. According to Irshad et al. (2013), the concentration of P in fresh cow manure is about 2500 mg/kg and about 1200 mg/kg in fresh goat manure. Fresh manure K amounts are about 9000 mg/kg for cow and about 10,000 mg/kg for goat, whereas Na levels are about 2000 and 2500 mg/kg, respectively. If the data of Irshad et al. (2013) are considered, the concentration in wt% for the respective oxides is as follows: for P_2O_5, cow = 0.57 and goat = 0.27; for K_2O, cow = 1.08 and goat = 1.20; and for Na_2O, cow = 0.27 and goat = 0.34. Since the mixing proportions of dung with clay are probably below the 50 wt%, it follows that the expected increase of concentration of such oxides is moderate.

The boxplots in Fig. 10 compare the P_2O_5 content of the different fabrics and show higher median for QVe potsherds and dispersion for QVe and QF. The pale grey zone shows the P_2O_5 range (0.03–0.29 wt%; median = 0.08) of the analysed sediments. In the inserted table are observable different correlations between P_2O_5 and CaO and between Na_2O and K_2O for each fabric. QVe and QKa samples show weak positive correlations, whereas Q samples show weak negative ones. The higher positive correlations of P_2O_5 with CaO and Na_2O in QVe compared to those of QKa demonstrate that the concentration of these oxides is not related to the same mineral components in the paste. The co-occurrence of short vegetal fibres and the correlated increase of P_2O_5, CaO, Na_2O and K_2O, compatible with the amounts of these oxides measured in fresh manure (Irshad et al. 2013), prove that fabric QVe was very likely tempered with livestock dung. According to dung origin and processing, the size of vegetal relics varies with the size of animals (Abbink 1999, p. 134); thus, the small size of the fibres could tentatively be attributed to ovicaprids (Van Neer et al. 2020) and/or to the pounding of hardened dung, before the mixing with clay. This is not the case in the samples of QF, where longer vegetal fibres were also identified, but their occurrence is not correlated to an increase of the aforementioned oxides. Moreover, from a technological point of view, dung addition probably allowed more workability of clay (Skibo et al. 1989), useful to get, for instance, thinner-walled vessels, as it is the case of Pastoral pottery production (§ 2.3), matching the occurrence of QVe fabrics' chronological distribution (Fig. 11). In fact, thin-walled sherds are mainly related to Q* fabrics, whereas QF* fabrics pertain to more thick-walled specimens and are more frequent in the earlier assemblages. The highest dispersion of P_2O_5 concentration among samples of fabric QF may be related to P contamination during use in different positions of the vessel (Rodrigues and da Costa 2016). The extreme values of P_2O_5 identified in TK32 (5.61 wt%) and TK33 (3.56 wt%) may be linked to the lying or use context as both have been excavated in what may have been a discard/midden or dump area where mixing with ash and other site maintenance materials is possible, though food processing cannot be excluded (Dunne et al. 2016).

In general, the porosity determined by DIA is underestimated because of the masking effect of the matrix on the porosity below 100 μm. Primary and secondary

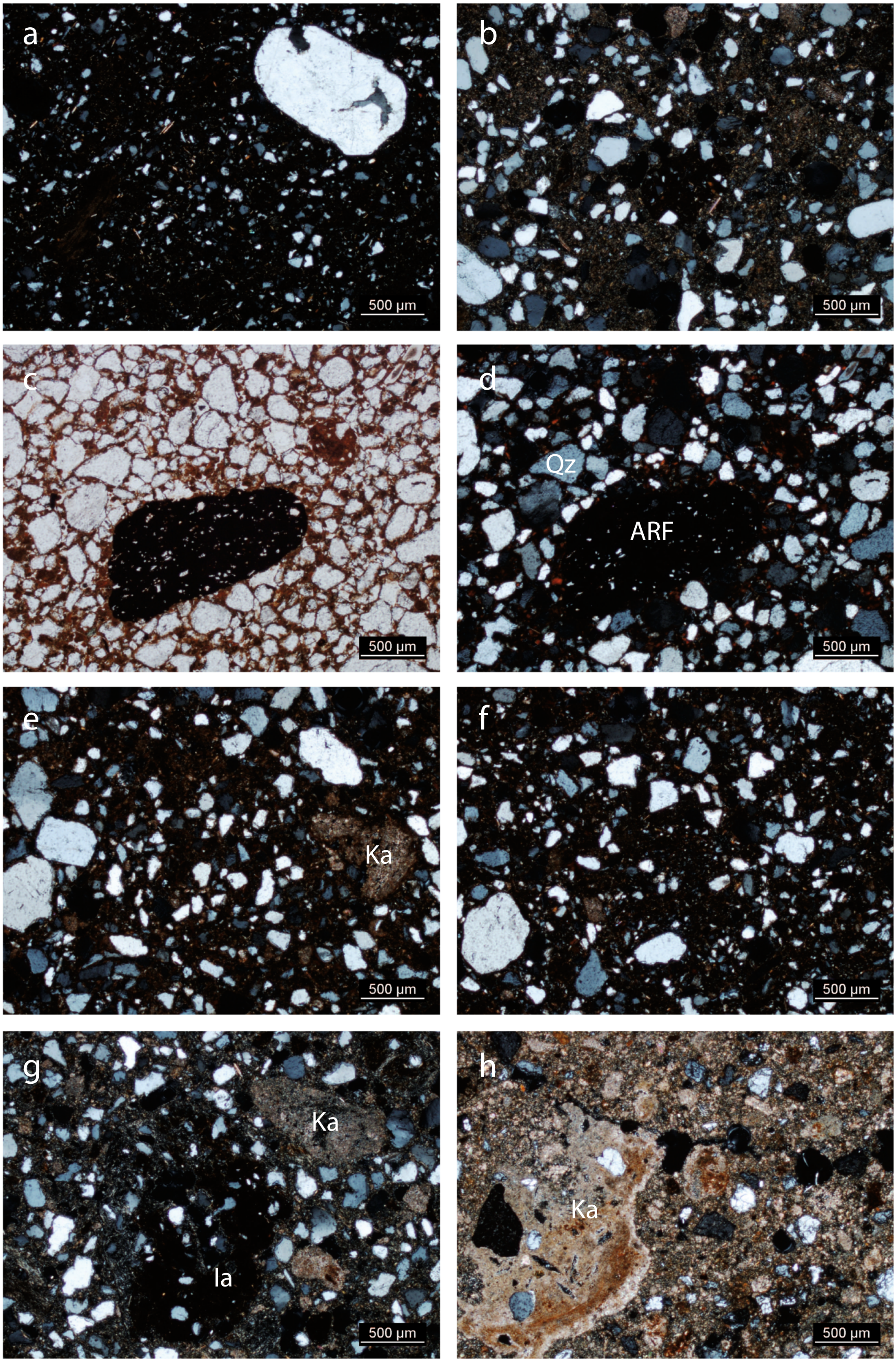

Fig. 7 Selected local sediments under the microscope. **a** TKS15a (2.5×, XP). **b** TKS15b (2.5×, XP). **c** TKS02 (2.5×, P). **d** TKS02 (2.5×, XP). **e** TKS04 (2.5×, XP). **f** TKS05 (2.5×, XP). **g** TKS10 (2.5×, XP). **h** TKS12 (2.5×, XP). Abbreviations as in Fig. 5

Table 13 Bulk chemical composition of local sediments by XRF

Sample	SiO_2	TiO_2	Al_2O_3	Fe_2O_3	MnO	MgO	CaO	Na_2O	K_2O	P_2O_5	LOI	Rb	Sr	Y	Zr	Nb
TKS01	93.08	0.31	4.01	1.58	0.01	0.17	0.14	0.05	0.27	0.04	1.26	9	31	8	216	6
TKS02	79.52	0.61	13.77	3.16	0.03	0.69	0.48	0.10	1.04	0.05	3.41	31	67	17	343	13
TKS03	90.27	0.37	5.92	1.70	0.02	0.42	0.27	0.10	0.54	0.06	1.38	17	46	10	238	8
TKS04	76.89	0.88	12.34	4.43	0.03	1.19	2.88	0.14	1.25	0.17	3.95	42	123	22	292	16
TKS05	75.81	1.04	13.09	5.11	0.08	1.20	2.55	0.21	1.43	0.22	4.15	50	121	24	248	18
TKS06	94.15	0.21	3.85	1.10	0.01	0.21	0.16	0.10	0.38	0.03	0.85	13	39	6	140	5
TKS07	91.20	0.32	5.26	1.67	0.01	0.32	0.16	0.08	0.43	0.03	1.41	15	43	8	207	7
TKS08	93.62	0.23	4.08	1.35	0.01	0.21	0.15	0.10	0.36	0.03	1.91	12	37	6	211	5
TKS09	92.73	0.26	5.01	1.50	0.02	0.49	0.28	0.09	0.45	0.05	1.15	15	43	7	212	7
TKS10	70.29	1.07	16.08	4.47	0.02	1.25	5.57	0.14	1.45	0.08	7.15	57	216	31	271	19
TKS11	86.33	0.61	8.85	2.53	0.03	0.62	0.42	0.16	0.93	0.08	3.11	27	64	14	259	12
TKS12	49.91	0.88	11.29	7.81	0.17	2.24	26.59	0.16	1.20	0.28	18.2	40	544	17	164	12
TKS13	92.73	0.25	3.42	1.23	0.01	0.31	1.54	0.12	0.37	0.04	0.98	12	51	7	293	6
TKS14	92.28	0.39	4.13	1.49	0.01	0.30	0.17	0.08	0.35	0.03	1.23	12	37	9	422	8
TKS15a	69.07	1.53	18.41	6.10	0.08	1.06	1.19	0.18	1.86	0.22	6.15	65	141	34	333	27
TKS15b	72.09	1.03	14.41	5.09	0.06	1.41	4.75	0.42	1.41	0.29	5.66	51	171	24	367	18
TKS15c	81.29	0.52	8.41	5.13	0.04	0.92	1.89	0.15	0.78	0.11	3.15	28	99	13	242	10
TKS17	52.87	1.20	12.84	6.23	0.32	10.15	13.02	0.08	2.68	0.04	14.95	75	68	53	592	21
TKS18	58.80	1.22	25.65	7.23	0.10	1.88	1.44	0.48	3.06	0.13	8.77	110	95	41	262	21
TKS19	60.98	1.04	23.74	6.56	0.06	2.55	0.62	0.84	2.66	0.15	7.90	92	101	28	334	18
TKS20	58.42	1.30	24.88	7.80	0.06	2.20	1.80	0.55	3.39	0.11	8.76	115	122	37	274	23
TKS21	69.22	0.82	20.37	5.06	0.05	1.35	0.75	0.42	2.12	0.15	5.16	68	89	21	272	13
TKS22	60.16	1.28	25.61	7.26	0.08	1.56	0.66	0.25	3.10	0.13	7.41	113	117	35	291	23

Concentrations of major and minor oxides and the LOI are expressed in wt% and those of trace elements in mg/kg

porosity is more frequent in QVe and Q fabrics, whereas secondary porosity is prevalent in QKa and QF fabrics (Table 5). The prevalence of samples with carbonaceous matter dispersed in the matrix mainly explains the secondary porosity

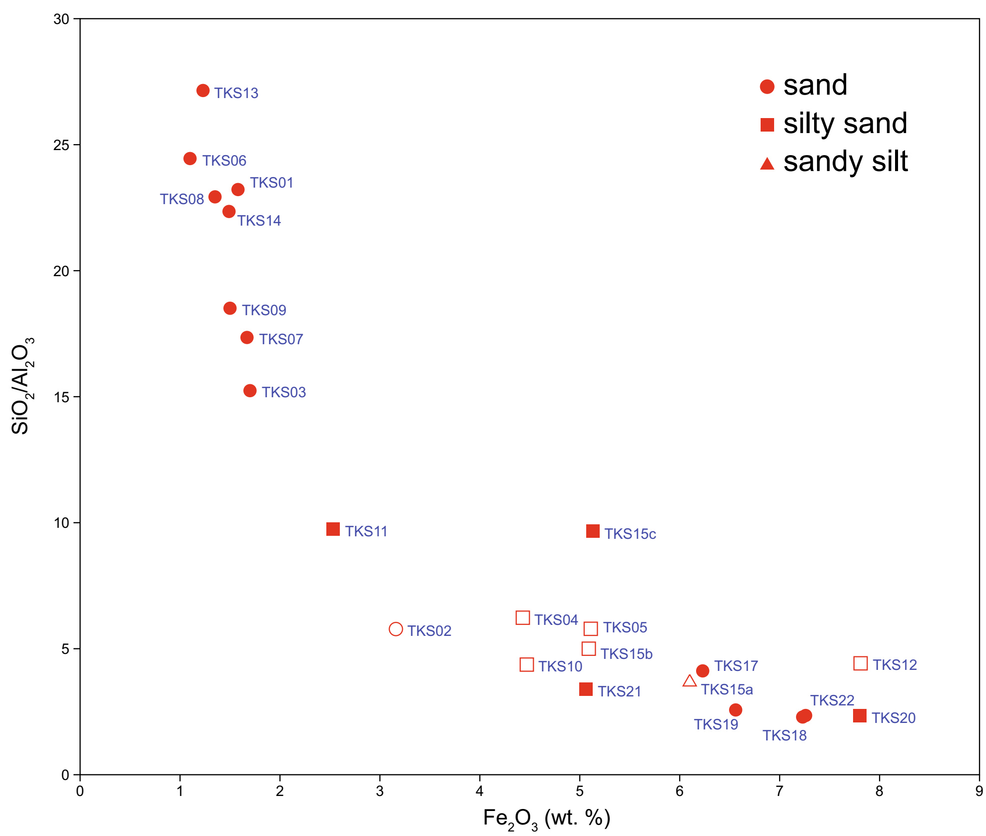

Fig. 8 Scatter plot of Fe_2O_3 vs. SiO_2/Al_2O_3 of the analysed sediments. Hollow symbols indicate the sediments used for the briquettes

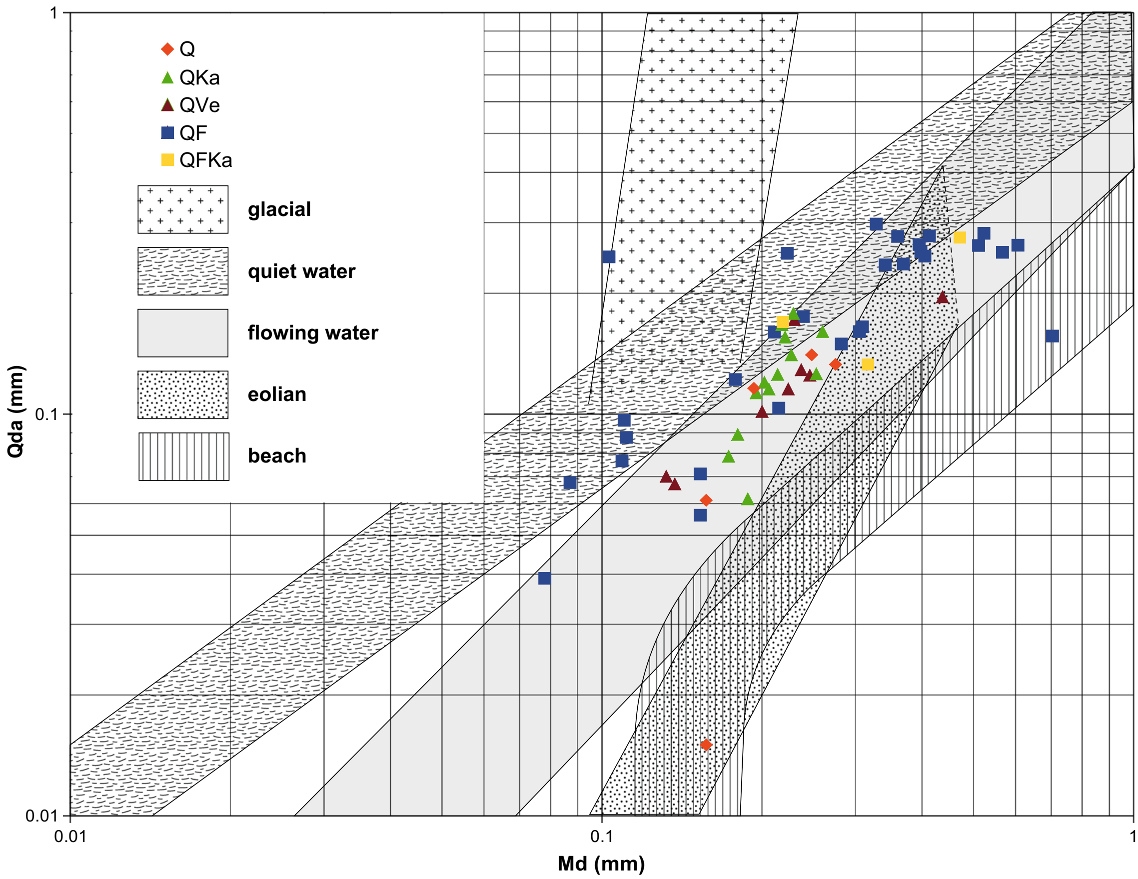

Fig. 9 A plot of the median grain size (Md) vs. the quartile deviation (Qda) of quartz inclusions (after Buller and McManus 1972) for the classification of sedimentary environments

formed during firing. The oxidation patterns of the potsherds point to firing modes dominated by reducing atmosphere with final oxidation of the surfaces during the cooling of the ceramic bodies (i.e. RO*). The mineralogical and microstructural analyses provide useful data indicating low to medium sintering degrees (Heimann and Maggetti 2014; Eramo and Mangone 2019). This points to EFTs between 500 and 800 °C for the QF* fabrics and to slightly higher EFTs for Q* fabrics (Table 5), well suited to open firings and compatible with the oxidation patterns observed in thin section (Gosselain 1992; Eramo and Mangone 2019). The diffused presence of primary and/or secondary porosity lowered the strength of the ceramic body but increased its thermal shock resistance and toughness (Tite et al. 2001; Allegretta et al. 2015).

Implication on mobility and pottery production

Our results point to various inferences related to pottery circulation and production within the long occupation of Takarkori. Figure 11 highlights a polarisation of frequency of the QF* fabrics in the Late Acacus and of the Q* fabrics in the Middle to Late Pastoral, with the Early Pastoral as a transition period, when the Q* fabrics appear. The local compositional fingerprint of Q* fabrics points to prevalent pottery production in the Takarkori area for the Middle Holocene periods of occupation, whereas the QF* fabrics suggest the local use of pottery produced with raw materials stemming from possible more distant areas.

All the fragments belonging to LA phase (but one: TK22) present fabrics with raw materials of allochthonous provenance, whose nearest known source is in the opposing southern edges of the Tassili n'Ajjer Formation, ca. 50 km away (Fig. 2). Excluding as more improbable, though not impossible, the movement or procurement of raw materials from sources located in an area far from the direct environs (> 30/50 km; Arnold 1988, pp. 32–60; Rice 2015) due to transportation issues (weight and quantities) over such distances, some of the pottery we are dealing with can be seen as introduced finished products, i.e. ceramic containers brought to the site. Several pots may have been transported from place to place in the system of residential mobility highlighted for this cultural horizon as part of the mobile and portable household assemblage, or raw materials collected from various and more distant sources were used for the realisation of the latter. The identification of granite-derived pottery fabrics of Late Acacus horizon in the site of Uan Tabu (Livingstone Smith 2001) is further evidence of sub-local provenance of some of the pottery in the Tadrart Acacus.

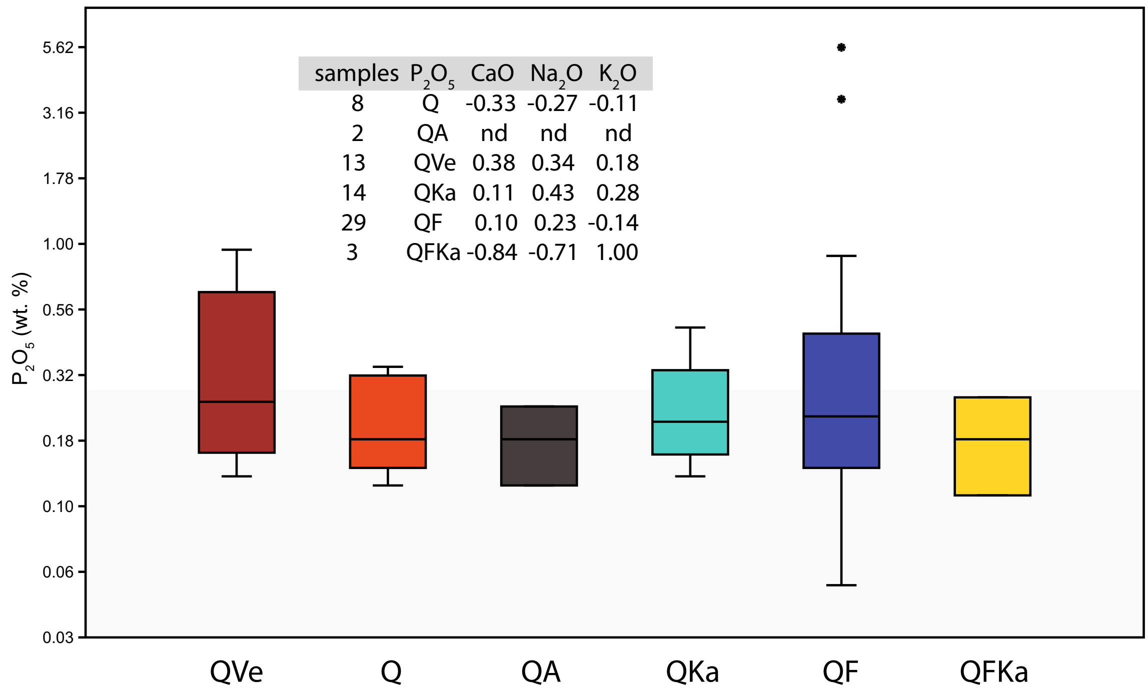

Fig. 10 Boxplots of the P_2O_5 content in the different fabrics. The pale grey zone shows the P_2O_5 range of the analysed sediments. Extreme outliers (> 3 IQR) are shown as stars. In the table, the values of the correlation coefficient (*r*) between P_2O_5 and CaO and between Na_2O and K_2O, for each fabric, are reported. The correlation (*r*) was not calculated for QA, because only two samples were available

It is by the way not difficult to imagine a wide home range of foraging communities in which seasonal movements were part of their settlement strategies. The presence of products realised with non-local raw materials may, therefore, be the witness of contacts and movements between HGF groups, all pertaining to a common cultural tradition. A tradition glimpsed in the extant common traits of the pottery production also in the other sites of the Tadrart Acacus and the Tassili with similar fabrics and decorative types (di Lernia 1999; Livingstone Smith 2001; Messili et al. 2013).

Bearing in mind that we should not a priori exclude a production with local raw materials, as highlighted by the presence of a specimen made of local clay, and possibly confined to some scant morpho-functional classes, the use of specific

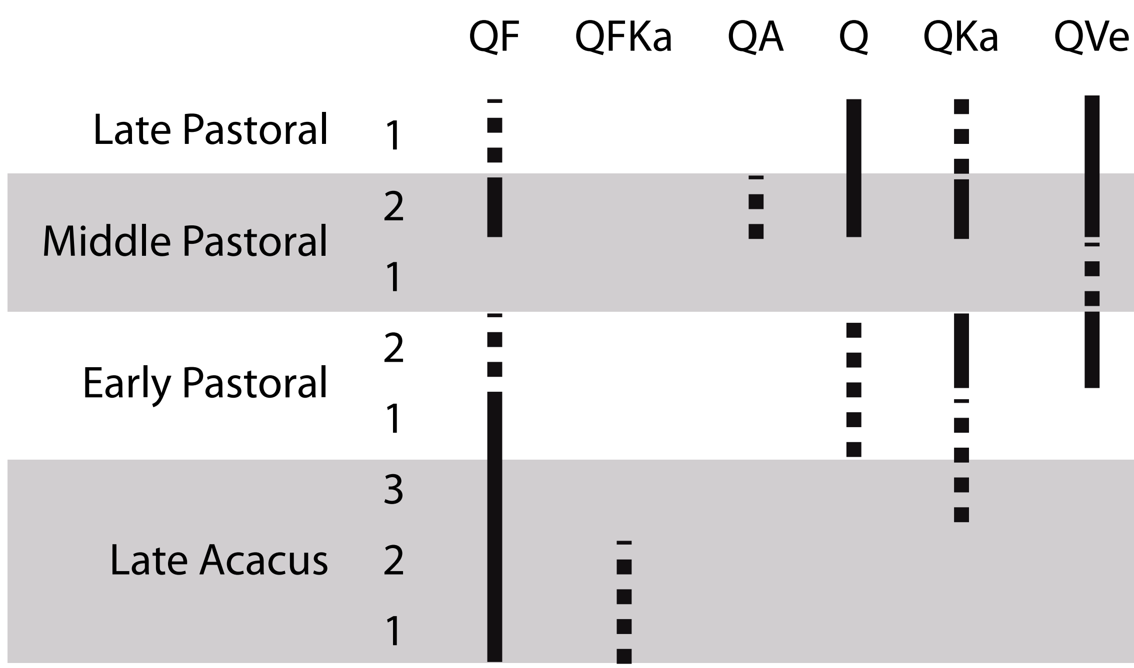

Fig. 11 Distribution of the pottery fabrics by cultural phases

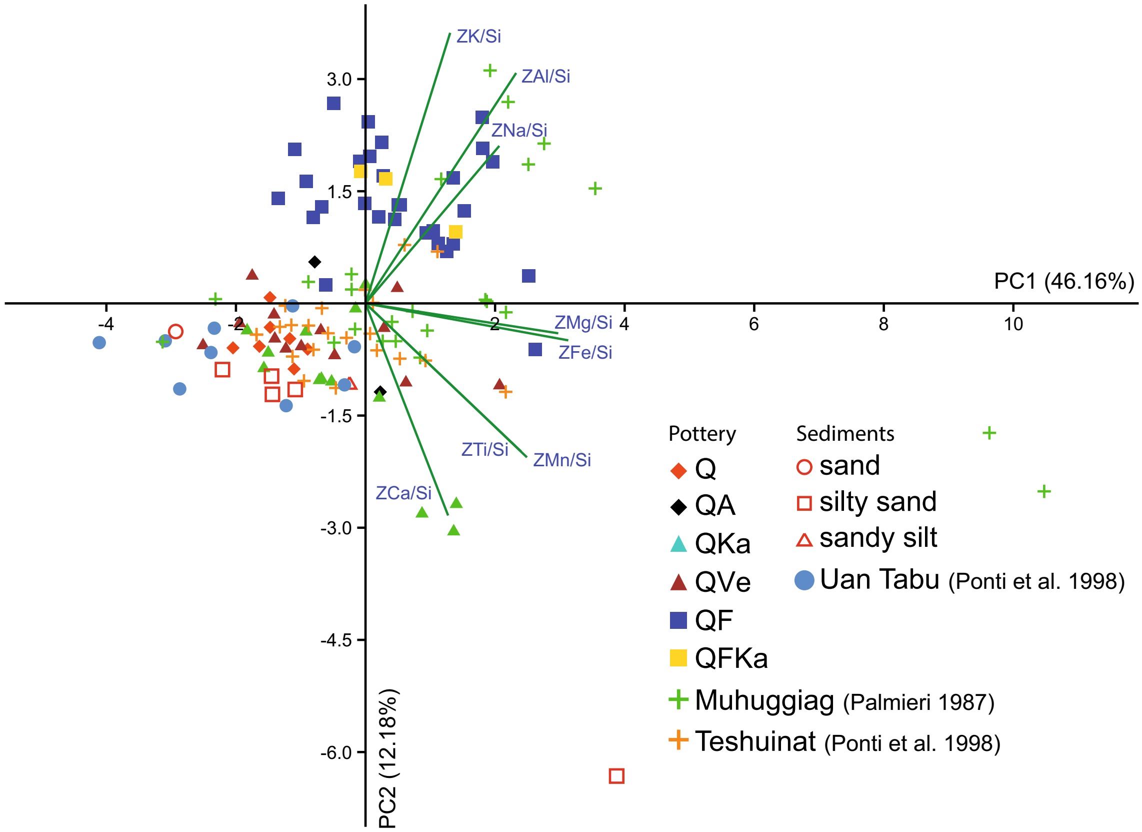

Fig. 12 Biplot diagram for the first two principal components related to the different pottery fabrics of Takarkori and the sediments studied here, compared with the bulk chemical data available in the literature. XRF data of pottery from Uan Muhuggiag ($n = 24$; Palmieri 1987) and pottery ($n = 22$) and local sediments (Uan Tabu, $n = 9$) from Wadi Teshuinat (Ponti et al. 1998)

materials, inclusions and pastes together with the extraordinary homogeneity of decoration patterns suggests precise choices of the individuals involved and entangled in a well-established technological and cultural tradition. These traits can be seen as a 'technical identity' that incorporates sets of *chaînes operatoires* (Leroi-Gourhan 1965; Livingstone Smith 2001; Roux 2019) expression of the potter's various social and behavioural boundaries, networks and identities (Gosselain 2000). Late Acacus pottery manufacture, in fact, has to be related to the cultural 'milieu' of the hunter–gatherer–fishers of the central Saharan massifs which indeed embrace at least the Tadrart Acacus and the Tassili n'Ajjer (Messili et al. 2013).

A somewhat different picture can be drawn for the subsequent Pastoral period, in which we see a much more diversified technological imprint with more varied clay pastes. Fabrics with local raw materials seem to predominate in the samples analysed, albeit allochthonous ones are present. Data referring to the Pastoral occupation may be interpreted as an indication of a more expedient pottery production, i.e. exploiting raw materials immediately achievable/reachable in the surroundings although in a highly mobile settlement pattern, fitting the needs of the main economic strategy. The local or sub-local raw material procurement can indeed be inserted in a wider cultural–behavioural reconstruction, in which pottery production becomes a matter related to more circumscribed domestic units. Groups probably split during certain times in the year occupying the mountainous areas of the Tadrart Acacus, in which domestic production activities were bounded to the exploitation of immediate local resources, in faster and lower time-consuming processes. Despite the employment of local and easily accessible resources, morphological and stylistic needs and outcomes were curated, inserted in a shared cultural tradition in which morpho-stylistic traits were wider-spread in space and time.

The high number of potsherds recovered from the site is clearly to assign to the palimpsest nature of the deposit, a result of different and prolonged occupations spanning several millennia.

The comparison between the bulk chemical data of the potsherds and sediments studied here with those of the potsherds and local sediments from Wadi Teshuinat (Ponti et al. 1998) and Uan Muhuggiag (Palmieri 1987) (Fig. 12) shows that most of these samples match the samples of Q* fabrics, whereas only a few samples of Uan Muhuggiag and Wadi Teshuinat match the samples of QF* fabrics. This occurrence testimonialises the exploitation of clay sources in the immediate environs and the local production, in particular, for the

Pastoral pottery assemblage, further corroborated by the close distribution of samples of Q* fabrics and the selected sediments of Takarkori and those of Uan Tabu.

Final remarks

The archaeometrical study of the pottery from Takarkori rock shelter and sediments from different areas close to the Tadrart Acacus massif allowed the understanding of classification, manufacture and provenance of vessels. The following main results were obtained:

- Two main fabric groups (i.e. Q* and QF*) were identified
- The selected sandy silts from Takarkori area are compatible with the Q* fabrics
- Pottery with plutonic NPIs (QF, QFKa) is incompatible with the quartz-dominated petrofacies of the local sediments of Takarkori and points to a probable provenance from the southern edges of Tassili n'Ajjer
- QF* fabrics are more frequent in Late Acacus and Early Pastoral layers, whereas Q* fabrics are more common during the Pastoral. Early Pastoral appears as a transition period
- Petrographical features point to the use of unprocessed clays, except for fabric QVe, where some dung was added, probably to make the sandy paste more plastic. Such technological choice is coupled with consolidated economic features (herding) of these later periods
- Results on ceramics point to a change of modes of pottery production and circulation in the Takarkori area through time: in the Late Acacus, ties with the nearby Tassili n'Ajjer are evident in ceramic manufacture and circulation (hunter–gatherer–fishers with residential mobility), while from EP2, the exploitation of local raw material sources in pottery production was more frequent (herders, shorter-stay occupations, expedient production).

Acknowledgements This research paper is part of the activities of 'The Archaeological Mission in the Sahara', Sapienza University of Rome and Department of Antiquities, Tripoli (Libya), directed by SDL. The excavations at Takarkori, including the sampling strategy, were designed and headed by SDL. The Department of Antiquities, Tripoli (Libya), granted all the necessary field and laboratory permissions to Sapienza University of Rome. We thank all our Libyan colleagues in Tripoli and Ghat. This research has been supported by Sapienza University of Rome (Grandi Scavi di Ateneo) and by the Minister of Foreign Affairs (DGSP - VI) with funds entrusted to SDL.

This study benefited of instrumental upgrades of 'Potenziamento Strutturale PONa3_00369 - Università degli Studi di Bari A. Moro', entitled 'Laboratorio per lo Sviluppo Integrato delle Scienze e delle TEcnologie dei Materiali Avanzati e per dispositivi innovativi (SISTEMA)'.

Author contributions SDL, GE and IMM conceived and designed the study. GE, SDL, IMM, RR and AZ wrote the paper. All the authors contributed to the manuscript with specific input: GE made the petrographical, mineralogical and chemical analyses of the potsherds and the petrographical analysis of the sediments; IMM started with the archaeometric analyses and made the comparison with previous published data; AA made the image analysis on potsherds; MP analysed the sediments; RR examined the pottery assemblage; AZ studied and reconstructed the climate, geologic and environmental context; and SDL provided the stratigraphic chronological and archaeological data. All authors contributed equally to the discussion and approved the final draft.

References

Abbink AA (1999) Make it and break it: the cycles of pottery. A study of the technology, form, function and use of pottery from the settlements at Uitgeest-Groot Dorregeest and Schagen-Muggenburg. PhD, Leiden University

Ali Kalefa El-ghali M (2005) Depositional environments and sequence stratigraphy of paralic glacial, paraglacial and postglacial Upper Ordovician siliciclastic deposits in the Murzuq Basin, SW Libya. Sediment Geol 177:145–173. https://doi.org/10.1016/j.sedgeo.2005.02.006

Allegretta I, Eramo G, Pinto D, Kilikoglou V (2015) Strength of kaolinite-based ceramics: comparison between limestone-and quartz-tempered bodies. Appl Clay Sci 116:220–230

Aprile A, Castellano G, Eramo G (2014) Combining image analysis and modular neural networks for classification of mineral inclusions and pores in archaeological potsherds. J Archaeol Sci 50:262–272

Aprile A, Castellano G, Eramo G (2019) Classification of mineral inclusions in ancient ceramics: comparing different modal analysis strategies. Archaeol Anthropol Sci 11:2557–2567. https://doi.org/10.1007/s12520-018-0690-y

Arnold DE (1988) Ceramic theory and cultural process. Cambridge University Press

Aumassip G (1984) Le site de Ti-n-Hanakaten et la néolithisation sur les marges orientales du Sahara central. Cahiers ORSTOM, Série Géologie 14:201–203

Barich BE (1974) La serie stratigrafica dell'uadi Ti-n-Torha (Acacus, Libia): per una interpretazione delle facies a ceramica saharo-sudanesi. Origini Preistoria e Protoistoria delle Civilta Antiche Roma 8:7–157

Barich BE (1987) The Wadi Ti-n-Torha facies. In: Archaeology and environment in the Libyan Sahara: the excavations in the Tadrart Acacus, 1978-1983. B.A.R., Oxford, pp 97–112

Biagetti S, di Lernia S (2013) Holocene deposits of Saharan rock shelters: the case of Takarkori and other sites from the Tadrart Acacus Mountains (southwest Libya). Afr Archaeol Rev 30:305–338

Buller AT, McManus J (1972) Simple metric sedimentary statistics used to recognize different environments. Sedimentology 18:1–21

Caneva I (1987) Pottery decoration in prehistoric Sahara and Upper Nile: a new perspective. In: Archaeology and environment in the Libyan Sahara: the excavations in the Tadrart Acacus, 1978-1983. B.A.R. International Series 368, Oxford, England, pp 231–254

Cherkinsky A, di Lernia S (2013) Bayesian approach to 14C dates for estimation of long-term archaeological sequences in arid environments: the Holocene site of Takarkori rockshelter, southwest Libya. Radiocarbon 55(02):771–782

Collomb P, Maggetti M (1996) Dissolution des phosphates présents dans des céramiques contaminées. ArchéoSciences, revue d'Archéométrie 20:69–75

Cremaschi M, Di Lernia S (eds) (1998) Wadi Teshuinat palaeoenvironment and prehistory in south-western Fezzan (Libyan Sahara). CNR, Milano

Cremaschi M, Zerboni A (2009) Early to Middle Holocene landscape exploitation in a drying environment: two case studies compared from the central Sahara (SW Fezzan, Libya). Compt Rendus Geosci 341:689–702

Cremaschi M, Zerboni A (2011) Human communities in a drying landscape: Holocene climate change and cultural response in the central Sahara. In: Martini IP, Chesworth W (eds) Landscapes and societies: selected cases. Springer Netherlands, Dordrecht, pp 67–89

Cremaschi M, Zerboni A, Spötl C, Felletti F (2010) The calcareous tufa in the Tadrart Acacus Mt. (SW Fezzan, Libya): an early Holocene palaeoclimate archive in the central Sahara. Palaeogeogr Palaeoclimatol Palaeoecol 287:81–94. https://doi.org/10.1016/j.palaeo.2010.01.019

Cremaschi M, Zerboni A, Mercuri AM, Olmi L, Biagetti S, di Lernia S (2014) Takarkori rock shelter (SW Libya): an archive of Holocene climate and environmental changes in the central Sahara. Quaternary Sci Rev 101:36–60

Davidson L, Beswetherick S, Craig J, Eales M, Fisher A, Himmali A, Jho J, Mejrab B, Smart J (2000) Chapter 14 - The structure, stratigraphy and petroleum geology of the Murzuq Basin, southwest Libya. In: Sola MA, Worsley D (eds) Geological exploration in Murzuq Basin. Elsevier Science B.V., Amsterdam, pp 295–320

Davis JC (1986) Statistics and data analysis in geology, John Wiley & Sons Inc

Deer WA, Howie RA, Zussman J (1992) An introduction to the rock-forming minerals: Essex, Longman Press, Pearson Education Limited

Dell'Anna L, Laviano R (1987) Analisi granulometrica di argille: esame dei principali metodi. In: Proceeding of the workshop "Procedure di analisi di minerali argillosi". ENEA, La Spezia. pp 215–234

Desio A (1937) Geologia e morfologia. Sahara Italiano Parte prima: Fezzán e Oasi di Gat 39–94

di Lernia S (1999) The Uan Afuda cave. Hunter-gatherer societies of central Sahara. All'Insegna del Giglio, Firenze

di Lernia S, Tafuri MA (2013) Persistent deathplaces and mobile landmarks: the Holocene mortuary and isotopic record from Wadi Takarkori (SW Libya). J Anthropol Archaeol 32:1–15. https://doi.org/10.1016/j.jaa.2012.07.002

di Lernia S, Massamba N'siala I, Mercuri AM (2012) Saharan prehistoric basketry. Archaeological and archaeobotanical analysis of the early-middle Holocene assemblage from Takarkori (Acacus Mts., SW Libya). J Archaeol Sci 39:1837–1853. https://doi.org/10.1016/j.jas.2012.01.026

Duistermaat K (2016) The organization of pottery production. In: Hunt A (ed) The Oxford handbook of archaeological ceramic analysis, p 114

Dunne J, Evershed RP, Salque M, Cramp L, Bruni S, Ryan K, Biagetti S, di Lernia S (2012) First dairying in green Saharan Africa in the fifth millennium BC. Nature 486:390–394

Dunne J, Mercuri AM, Evershed RP, Bruni S, di Lernia S (2016) Earliest direct evidence of plant processing in prehistoric Saharan pottery. Nature Plants 3:1–6. https://doi.org/10.1038/nplants.2016.194

Edwards MG (1916) Introduction to optical mineralogy and petrography-the practical methods of identifying minerals in thin section with the microscope and the principles involved in the classification of rocks. Camp, Cleveland

Eramo G, Mangone A (2019) Archaeometry of ceramic materials. Phys Sci Rev 4. https://doi.org/10.1515/psr-2018-0014

Eramo G, Aprile A, Muntoni IM, Zerboni A (2014) Textural and morphometric analysis applied to Holocene pottery from Takarkori rock shelter (SW Libya, central Sahara): a quantitative sedimentological approach. Archaeometry 56:36–57. https://doi.org/10.1111/arcm.12043

Franzini M (1975) Revisione di una metodologia analitica per fluorescenza-X, basata sulla correzione completa degli effetti di matrice. Rend Soc Ital Miner Petrol 31:365–378

Franzini M, Leoni L, Saitta M (1972) A simple method to evaluate the matrix effects in X-ray fluorescence analysis. X-Ray Spectrom 1: 151–154. https://doi.org/10.1002/xrs.1300010406

Galeĉiĉ M (1984) Geological map of Libya, explanatory booklet, sheet: Anay, NG 32-16, scale 1: 250000. Industrial Research Centre, Tripoli

Garcea EAA (2001) Uan Tabu in the settlement history of the Libyan Sahara. All'Insegna del Giglio, Firenze

Gasse F (2000) Hydrological changes in the African tropics since the Last Glacial Maximum. Quaternary Sci Rev 19:189–211. https://doi.org/10.1016/S0277-3791(99)00061-X

Gatto MC (2002) Early Neolithic pottery of the Nabta-Kiseiba area: stylistic attributes and regional relationships. In: Nelson K (ed) Holocene settlement of the Egyptian Sahara: the pottery of Nabta Playa, vol 2. Kluwer Academic/Plenum, New York, pp 65–78

Gosselain OP (1992) Bonfire of the enquiries. Pottery firing temperatures in archaeology: What for? J Archaeol Sci 19:243–259

Gosselain OP (2000) Materializing identities: an African perspective. J Archaeol Method Th 7:187–217

Hammer O, Harper DAT, Ryan PD (2001) PAST: Paleontological Statistics software package for education and data analysis. Palaeontol Electron 4:9

Heimann RB, Maggetti M (2014) Ancient and historical ceramics: materials, technology, art and culinary traditions. Schweizerbart Science, Stuttgart

Irshad M, Eneji AE, Hussain Z, Ashraf M (2013) Chemical characterization of fresh and composted livestock manures. J Soil Sci Plant Nut 13:115–121. https://doi.org/10.4067/S0718-95162013005000011

Jakovljevic Z (1984) Geological map of Libya, 1: 250,000. Sheet: Al Awaynat NG 32-12. In: Explanatory booklet. Industrial Research Centre Tripoli, Libya, p 140

Jesse F (2010) Early pottery in Northern Africa – an overview. J Afr Archaeol 8:219–238. https://doi.org/10.3213/1612-1651-10171

Kulkova M, Kulkov A (2016) The identification of organic temper in Neolithic pottery from Russia and Belarus. The Old Potter's Almanack 21:2–12

Leoni L, Saitta M (1976) Determination of yttrium and niobium on standard silicate rocks by X-ray fluorescence analyses. X-Ray Spectrom 5:29–30. https://doi.org/10.1002/xrs.1300050107

Leroi-Gourhan A (1965) Le Geste et la Parole-: La mémoire et les rythmes. Albin Michel, Paris

Livingstone Smith A (2001) Pottery manufacturing processes: reconstruction and interpretation, in Uan Tabu in the settlement history of the Libyan Sahara. In: Garcea EAA (ed) Uan Tabu in the settlement history of the Libyan Sahara. All'Insegna del Giglio, Firenze, pp 113–152

London G (1981) Dung-tempered clay. J Field Archaeol 8:189–195

Maggetti M (1982) Phase analysis and its significance for technology and origin. In: Franklin AD, Olin JS (eds) Archaeological ceramics. Smithsonian Institution, Washington, pp 121–133

Matson FR (ed) (1965) Ceramics and man. Aldine, Chicago

McDougall N, Martin M (2000) Facies models and sequence stratigraphy of Upper Ordovician outcrops in the Murzuq Basin, SW Libya. In: Sola MA, Worsley D (eds) Geological exploration in Murzuq Basin. Elsevier Science B.V., Amsterdam, pp 223–236

Mercuri AM (2008) Human influence, plant landscape evolution and climate inferences from the archaeobotanical records of the Wadi Teshuinat area (Libyan Sahara). J Arid Environ 72:1950–1967. https://doi.org/10.1016/j.jaridenv.2008.04.008

Mercuri AM, Fornaciari R, Gallinaro M, Vanin S, di Lernia S (2018) Plant behaviour from human imprints and the cultivation of wild cereals in Holocene Sahara. Nature Plants 4:71–81. https://doi.org/10.1038/s41477-017-0098-1

Messili L, Saliège J-F, Broutin J, Messager E, Hatté C, Zazzo A (2013) Direct 14 C dating of early and mid-Holocene Saharan pottery. Radiocarbon 55:1391–1402

Munsell Color Company (1975) Munsell soil colour charts. Macbeth Division of Kollmorgen, Baltimore
Olmi L, Mercuri AM, Gilbert MTP, Biagetti S, Fordyce S, Cappellini E, Massamba N'siala I, di Lernia S (2011) Morphological and genetic analyses of early-mid Holocene wild cereals from the Takarkori rockshelter (central Sahara, Libya): first results and prospects. In: Windows on the African past. Current approaches to African archaeobotany. Africa Magna, Cairo, pp 175–184
Palmieri AM (1987) Chemical analysis of the Acacus pottery: a preliminary essay. In: Archaeology and environment in the Libyan Sahara: the excavations in the Tadrart Acacus, 1978-1983. B.A.R., Oxford, pp 221–229
Ponti R, Aurisicchio G, Damiotti R, Guidi G, Cremaschi M, di Lernia S (1998) Pottery from the Tadrart Acacus (Libyan Sahara): decoration, distribution and manufacture. Wadi Teshuinat Palaeoenvironment and prehistory in South-Western Fezzan (Libyan Sahara). Quaderni di Geodinamica Alpina e del Quaternario 7:183–200
Ramsey CB, Lee S (2013) Recent and planned developments of the program OxCal. Radiocarbon 55:720–730
Rice PM (2015) Pottery analysis: a sourcebook. University of Chicago Press, Chicago
Rodrigues SFS, da Costa ML (2016) Phosphorus in archeological ceramics as evidence of the use of pots for cooking food. App Clay Sci 123:224–231. https://doi.org/10.1016/j.clay.2015.10.038
Roset J-P (1996) La céramique des débuts de l'Holocène au Niger nord-oriental. Nouvelles datations, bilan des recherches. In: Aumassip G, Desmond Clark J, Mori F (eds) The prehistory of Africa. Abaco edizioni, Forlì, pp 175–182
Roux, V. (2019). Ceramics and society: a technological approach to archaeological assemblages. Springer
Rye OS (1981) Pottery technology: principles and reconstruction, vol 4. Taraxacum, Washington, DC
Shahack-Gross R (2011) Herbivorous livestock dung: formation, taphonomy, methods for identification, and archaeological significance. J Archaeol Sci 38:205–218. https://doi.org/10.1016/j.jas.2010.09.019
Shepard FP (1954) Nomenclature based on sand-silt-clay ratios. J Sediment Petrol 24:151–158. https://doi.org/10.1306/D4269774-2B26-11D7-8648000102C1865D
Sillar B, Tite MS (2000) The challenge of 'technological choices' for materials science approaches in archaeology. Archaeometry 42:2–20
Skibo JM, Schiffer MB, Reid KC (1989) Organic-tempered pottery: an experimental study. Am Antiq 54:122–146
Štorch P, Massa D (2006) Middle Llandovery (aeronian) graptolites of the Western Murzuq Basin and Al Qarqaf Arch region, south-west Libya. Palaeontology 49:83–112. https://doi.org/10.1111/j.1475-4983.2005.00530.x
Tite MS (1995) Firing temperature determinations how and why? In: Lindborgh A, Stilborg O (eds) The aim of Laboratory analysis of Ceramic inArchaeology, April 7–9, 1995, in Lund: Sweden, in Honor of Birgitta Huthen. Stockholm, Kungl. Vitterhets historie och antikvitets akademien, pp 37–42
Tite MS, Kilikoglou V, Vekinis G (2001) Strength, toughness and thermal shock resistance of ancient ceramics, and their influence on technological choice. Archaeometry 43:301–324
Traut MW, Boote DRD, Clark-Lowes DD (1998) Exploration history of the Palaeozoic petroleum systems of North Africa. Geol Soc Lond, Spec Publ 132:69–78. https://doi.org/10.1144/GSL.SP.1998.132.01.03
Tsetlin YB (2003) Organic tempers in ancient ceramics. In: Serneels V, Di Pierro S, Maggetti M (eds) Ceramics in the society. Proceedings of the 6th European Meeting on Ancient Ceramics, Fribourg. pp 289–306
van Doosselaere B, Delhon C, Hayes E (2014) Looking through voids: a microanalysis of organic-derived porosity and bioclasts in archaeological ceramics from Koumbi Saleh (Mauritania, fifth/sixth–seventeenth century AD). Archaeol Anthropol Sci 6:373–396. https://doi.org/10.1007/s12520-014-0176-5
Van Neer W, Alhaique F, Wouters W, Dierickx K, Gala M, Goffette Q, Mariani GS, Zerboni A, di Lernia S (2020) Aquatic fauna from the Takarkori rock shelter reveals the Holocene central Saharan climate and palaeohydrography. PLoS One 15(2)
Walter H, Lieth H (1960) Klimadiagramm. Wetatlas VEB Gustaf Fischer, Berlin
Wendorf F, Karlén W, Schild R (2007) Middle Holocene environments of North and East Africa, with special emphasis on the African Sahara. In: Anderson DG, Maasch KA, Sandweiss DH (eds) Climate change and cultural dynamics. Academic, San Diego, pp 189–227
Whitney DL, Evans BW (2010) Abbreviations for names of rock-forming minerals. Am Mineral 95:185–187. https://doi.org/10.2138/am.2010.3371
Zerboni A, Perego A, Cremaschi M (2015) Geomorphological map of the Tadrart Acacus massif and the Erg Uan Kasa (Libyan central Sahara). J Maps 11:772–787. https://doi.org/10.1080/17445647.2014.955891